The Thermal Stability of Carbon Materials in the Air: Quantitative Determination and Decisive Structural Parameters

Galina Sádovská[1,2], Pavla Honcová[2], Jaroslava Morávková[1], Ivan Jirka[1], Maryna Vorokhta[3], Radim Pilař[1], Jiří Rathouský[1], Dalibor Kaucký[1], Eliška Mikysková[1], Petr Sazama[1*]

[1]J. Heyrovsky Institute of Physical Chemistry, Academy of Sciences of the Czech Republic, Dolejskova 2155/3, 182 23 Prague, Czech Republic, [*]Corresponding author: petr.sazama@jh-inst.cas.cz

[2]Department of Inorganic Technology, Faculty of Chemical Technology, University of Pardubice, Doubravice 41, 532 10 Pardubice, Czech Republic

[3]Department of Geochemistry, Institute of Rock Structure and Mechanics, Czech Academy of Sciences, V Holesovickach 94/41, 18209 Prague 8, Czech Republic

Abstract

The variability of the nanostructure of carbon materials results in a uniquely wide range of physical and chemical properties. This work analyses how the nanostructure affects the thermal stability of 2D and 3D graphene-based materials (graphene, fullerene, nanotubes, and zeolite-templated carbon), disordered and 3D ordered mesoporous carbon materials (activated carbons, CMK-3, 3DOMM), and layered carbon materials (few-layer graphene, graphene nanoplatelets, graphite) in the air. The combination of structural, thermogravimetric and calorimetric analysis under identical conditions for all the carbon nanomaterials showed that the most decisive factor increasing the stability is the stacking of graphene layers parallel to each other with a long-range order, increasing the onset oxidation temperature (T_{on}) with the number of graphene layers from 530 °C for graphene up to 800 °C for graphite. The unsaturated carbon atoms at the defects and edges and the bending stress in the 3D graphene layers cause that graphene, the 3D non-defective monolayer in fullerenes and the defective monolayer in zeolite-templated carbon exhibit similar stability to disordered amorphous materials, as well as 3D organised mesoporous materials. All these materials are oxidised in a narrow interval T_{on} from 485 to 530 °C. The most significant factor for reducing the stability is the presence of specific oxygen-containing functional groups, lowering T_{on} for materials with oxidized edges with prevailing hydroxyl groups by up to 150 °C. The relationships between the carbon structure and the stability in the air provide information for targeting the nanostructure of carbon materials in relation to their stability.

Keywords: Nanostructured carbon materials; Carbon nanomaterials; Oxidation; Structure-stability relationship, Differential Scanning Calorimetry (DSC); Thermogravimetric analysis (TG)

1. Introduction

Carbon chemistry enables the preparation of nanostructured carbon materials with a wide range of physical properties that can be specifically targeted for the development of stable catalysts, electrocatalysts, adsorbents, sensors, and many other applications with enhanced functionality compared to traditional carbon materials. Traditional carbon materials such as graphite and activated carbons constitute the main group of materials that have been used for decades as catalyst supports in heterogeneous catalysis, and the use of nanostructured carbon materials can significantly improve their functionality [1-3]. However, the thermal stability of carbon nanomaterials in the air, e.g. nanocarbon catalysts for selective oxidation or oxidative dehydrogenation of hydrocarbons, is a prerequisite for their application [4-6]. The stability of carbon nanomaterials also plays a key role in their safe applications in electrodes in batteries, in electrochemical processes [7, 8] and in electronics [9]. The stability of nanocarbon materials is also used for enhancement of the functional properties of a broad range of nanocomposites [10].

The thermal behaviour and stability of carbon nanomaterials in the air have often been studied in detail for individual nanostructured carbon materials, such as nanotubes [6, 11-15], fullerenes [16-20], graphene and graphene-related materials [21-27]. However, the stability analysis is often based on various parameters of thermal investigation, such as the gas atmosphere, heating rate, and regime and the amount and form of the nanostructured analysed carbon, tailored for the requirements of their respective fields of application, and thus makes it difficult to compare the published results on the stability of nanostructured carbon materials. Even for precisely defined structures, such as C_{60} fullerene, a wide range of temperatures have been reported for oxidation in an oxidizing atmosphere. Oxidation of fullerene C_{60} was observed, e.g. at 450 °C by Gallagher and Zhong [19] and at 580 °C by Milliken et al. [16]. Later, Cuesta et al. showed that the thermal behaviour and stability of C_{60} fullerene depend on the heating rate because of the overlapping of different phenomena that take place during heating in an oxidizing atmosphere [28]. The stability of nanostructured carbon materials can be affected by the presence of other carbon phases, impurities, and imperfect structures, but also significantly by the measuring conditions of the thermal analysis. Analyses of the thermal stability of nanotubes have found their oxidation in a wide temperature range from 350 °C to 600 °C depending on the measuring conditions, the amorphous carbon content present in the nanotube samples [13, 29] and the transition metal catalyst content used for preparation of the nanotubes [13, 29, 30]. The maximum and end oxidation temperatures of carbon nanotubes were also shown to be strongly affected by different heating rates [31].

In this study, the potential and advantages of thermal analysis were exploited for determining the stability of important representatives of traditional and nanostructured carbon materials . The study was not directed towards gaining an understanding of all the structural parameters affecting the stability at the atomic level, but rather towards describing and directly comparing the thermal stability of important carbon nanostructures, considering their structural order and degree and type of defects characterising the individual groups of nanostructured carbon materials. Four groups of carbon materials were investigated in this study: i) Planar carbon materials with different numbers of graphene layers (graphene, double-layer graphene (2LG), graphene nanoplatelets (GNPs) and graphite), ii) oxidized carbon materials with a single layer (oxidized single-walled nanotubes (Ox-SWNTs)) and multiple graphene layers (oxidized double-layer graphene (Ox-2LG), oxidized graphene nanoplatelets (Ox-GNPs) and graphite oxide (GtO)), iii) 3D carbon materials with a single carbon layer (fullerenes C_{60} and C_{70} and zeolite-templated carbon (*Y*-carbon)), and iv) amorphous carbon materials (activated carbons (AC) and 3D organized mesoporous carbon materials (3DOMM and CMK-3)). Illustrations of the structures of the studied carbon materials are shown in Figure 1. These four types of materials were chosen to analyse the effect of different numbers of graphene layers, the presence of oxygen-containing functional groups, the 3D organization of graphene layer and structural disorder on the thermal stability in the air. The structure of the studied materials was described using complementary microscopic, diffraction, sorption and spectroscopic techniques, and then their thermal stability was analysed to identify the decisive structure-stability relationships. The work demonstrates how the nanostructure affects the stability under identical conditions, providing a knowledge base for rational choice of conditions during the preparation of functional carbon nanomaterials and conditions for their possible use with respect to their stability.

2. Experimental

2.1 Carbon Materials

This study preferably employed readily available standard carbon materials to analyse their stability in the air. Materials that are not commonly commercially available were synthesized in our laboratory using well-established procedures. Graphene (PN AC453150010, LN A0443419) was provided by Thermo Scientific. Graphene (2-3 layers, LN GP043-18) was supplied by 2DM. Graphene nanoplatelets (PN 799084, LN MKCC1502), Oxidised graphene nanoplatelets (PN 796034, LN MKCP6914), Graphite (PN 1.04206, LN MKBV3964), oxidised single-walled carbon nanotubes (PN 775533, LN MKCM0030), fullerene C_{60} (PN

572500, LN WXBD5649V), fullerene C_{70} (PN 482994, LN MKCB3512), activated carbons (PN 31616, BCCG4825 and PN 1.02184, LN K52167084 138) were purchased from Sigma-Aldrich. The CMK-3 carbon material characterised by a two-dimensional hexagonal rod array was synthesized using furfuryl alcohol (FA, 98%, Sigma-Aldrich) as the carbon precursor and ultra-large-pore mesoporous SBA-15 silica was used as the hard template. The pores of SBA-15 silica were impregnated with a mixture of FA and oxalic acid dihydrate (OAD, 99%, Sigma-Aldrich) keeping the FA/SiO_2 ratio at 4.4 and annealed at a FA polymerisation temperature of 90 °C for 4 days and at 150 °C for 3 h. The composite material was then pyrolyzed at a temperature of 900 °C for 3 h. SiO_2 was removed in 5% hydrofluoric acid (HF) for 5 h and then for 40 min in 40% HF at room temperature. A detailed description of the synthesis of CMK-3 is published elsewhere [32]. 3DOMM carbon with a spherically porous three-dimensionally ordered micro-mesoporous structure was prepared using SiO_2 nanoparticles according to Fan et al. [33]. The lysine-silica nanoparticle solution was evaporated and then dried at 70 °C. The space among the prepared SiO_2 nanoparticles was filled with a mixture of FA and OAD. The composite material was pyrolyzed at 900 °C for 3 h and cooled in a flowing helium atmosphere. The silica spheres were dissolved in a large excess of 5% HF aqueous solutions for 5 h and in 40% HF solutions for 40 min at room temperature. 3DOMM carbon was repeatedly washed with demineralized water and filtered [34]. Zeolite-templated carbon (*Y*-carbon) was prepared using faujasite (FAU) zeolite (H^+ form, Si/Al = 6, Zeolyst Int., PN CBV712, LN 712014001708,) as a hard template. Chemical vapor deposition with propylene at 750 °C and subsequent calcination in a He stream at 900 °C was carried out to form the 3D graphene-like structure in the zeolite channels. The zeolite matrix was subsequently dissolved with HF and HCl acids. The resulting 3D nanocarbon sample was isolated by repeated centrifugations, washed with a large volume of demineralized water, and filtered. Finally, the *Y*-carbon sample was dried in the air at 120 °C for 12 h. For a detailed description of the *Y*-carbon, see Ref. [3].

2.2 Characterization of Carbon Materials

High resolution transmission electron microscopy (HR-TEM) analysis was carried out using a JEOL JEM 2100 instrument with accelerating voltage of 200 kV, an La-B_6 filament as an electron source and resolution of the lattice image of 0.14 - 0.2 nm. The samples were dispersed in ethanol and a droplet of dispersion was cast on a lacey carbon coated copper grid specimen support. A low sample concentration in the dispersion was used to avoid an excessive agglomeration during evaporation. Microscopic images were taken for the particles of the

studied carbon material captured and randomly oriented on the edge of the holes of the lacey carbon film. This enables TEM measurement without background interference. The measurement of 60 nanoplatelets was carried out and the ImageJ software was used for estimation of the number of layers in carbon nanoplatelets. The crystalline structure was studied by X-ray diffraction (XRD). The results were collected using a MiniFlex600 diffractometer (Rigaku) working in Brag-Brentano ($\theta/2\theta$) geometry with a 1D D/teX Ultra silicon strip detector and Kβ filter. $CuK_{\alpha 1}$ ($\lambda = 0.15418$ nm) and $CuK_{\alpha 2}$ ($\lambda = 0.15405$ nm) radiation were used. The diffractograms were obtained for an angle of 2θ in the range from 2° to 80°, step size 0.01°, with a data collection speed of 5° min^{-1}. The porosity of the carbon materials was determined by nitrogen adsorption at the boiling temperature of liquid nitrogen. Before the adsorption experiments, the samples were degassed at 240 °C for at least 24 h to ensure complete surface cleaning. The experiments were performed using an ASAP2010 instrument (Micromeritics). GtO was degassed at 80 °C for 24 h because it is unstable and can undergo decomposition at temperatures above 140 °C [35, 36]. The BET (Brunauer-Emmett-Teller) theory was used to evaluate the total surface areas. The porosity distribution was evaluated by the Density Functional Theory using the N_2 - DFT Model with non-negative regularization. An Omicron Nanotechnology ESCAProbe P spectrometer (Omicron Nanotechnology GmbH, Taunusstein) was used to measure the X-ray photoelectron spectra. XPS analysis was performed at a pressure of ~10^{-8} Pa. The X-ray source was monochromatic at 1486.6 eV. The XPS spectra were measured with a step size of 0.1 eV. A damped nonlinear least-squares fitting procedure was used to distinguish partially resolved lines in the C 1s photoelectron spectra [37]. The spectra were approximated by a weighted sum of a minimal number of lines approximated by pseudo-Voight functions. The Shirley background was employed.

2.3 Analysis of Thermal Stability

The thermal stability was analysed using simultaneous thermogravimetry and differential scanning calorimetry (TG-DSC, Labsys, Setaram). The temperature and the calorimetric signal of the instrument were calibrated using pure metals (In, Sn, Pb, Zn, Al, Ag, Au, and Ni). The noise level was 0.002 mg for the TG signal and 0.2 mW for the DSC signal. The 5 mg samples were measured within the 25 – 1200 °C temperature range in a corundum crucible (volume 100 μl) with a heating rate of 10 °C min^{-1}. The experiments were carried out under an atmosphere of synthetic air (mixture of 20% pure oxygen in pure nitrogen, Messer Technogas) with a flow rate of 50 ml min^{-1}. The measurement curves were corrected by performing an automatic blank curve subtraction. The blank curves were measured with an

empty crucible. Both the sample weight loss and the heat flow were analysed as functions of the temperature. The TG signal was evaluated as the change in the sample mass Δm (%) over a certain temperature range. The characteristic onset (T_{on}), maximum (T_{max}), and offset (T_{off}) temperatures were determined from the DSC signals (see the evaluation description in Figure S1). The reproduced TG/DTG-DSC measurements are shown in Figure S2.

3. Results and Discussion

3.1. Analysis of the Structure of Carbon Materials

The study compares the thermal stability of materials with a planar structure but with different numbers of graphene layers (graphene, 2LG, GNPs and graphite), oxidized carbon materials (Ox-2LG, Ox-SWNTs, Ox-GNPs and GtO), 3D carbon materials with a single graphene layer (fullerenes C_{60} and C_{70} and *Y*-carbon), and amorphous activated and 3D organized mesoporous carbon materials (AC, 3DOMM and CMK-3). Illustrations of the structures of the studied carbon materials and their structural characteristics are shown in Figure 1 and Table 1. The structures of all materials were analysed using complementary microscopy (HR-TEM, HR-SEM), XRD, XPS, and N_2 sorption characterization techniques prior to calorimetric and thermogravimetric analysis of the stability.

3.1.1. Microscopic Analysis

Representative HR-TEM images of the studied carbon materials are shown in Figure 2. The HR-TEM images of graphene and oxidized graphene appear as almost transparent, slightly wavy and crumpled, variously interwoven sheets characteristic of suspended graphenes [38]. In addition to the characteristic graphene monolayers, regions with the presence of several stacked graphene layers (typically 2-3, rarely 4-5) with extended lateral dimensions were also observed in a very small number in the samples. The images of 2-LG materials show the presence of typically two to three layers with a small occurrence of multiple layers and a lateral size of sheets up to 1 μm. The microscopic images of GNPs and Ox-GNPs contain submicrometer platelets consisting of several sheets of graphene with an overall thickness of 5 - 20 layers (Figure S3). Characteristic TEM images of graphene, Ox-2LG and graphene nanoplatelets at the same magnification in figure S4 clearly show the difference in the shape of single and multilayer materials. While graphene materials resemble crumpled silk, multilayer graphene nanoplatelets are in the form of planar plates. Microscopic images of graphite exhibit the characteristic graphite structure consisting of regularly stacked layers of graphene forming large units of graphite grains.

Microscopic analysis of the sample of single-walled nanotubes indicated the presence of well-developed nanotubes with various diameters (0.8 –1.7 nm) and a small admixture of amorphous material (Figure 2). The microscopic images of C_{60} and C_{70} fullerenes depicts the presence of characteristic spherical molecules with diameters of 0.7 nm and 0.78 nm, respectively. The spherical particles of fullerenes are regularly arranged by agglomeration in such a way that the image gives the impression of a crystalline material of large dimensions with long-range order (Figure 2). The agglomeration of the hollow spheres of the C_{60} and C_{70} molecules is typical for powdered fullerenes [39]. The image of *Y*-carbon exhibits a well-ordered structure with the external crystal morphology of the zeolite template and lattice fringes indicating replication of the channel system of the zeolite in the carbon material [3].

The microscopy image of activated carbon in Figure 2 depicts a material without any regular organization typical of an amorphous matrix of activated carbon [40]. TEM images of the 3DOMM and CMK-3 carbon materials demonstrate a three-dimensionally ordered mesoporous structure with the characteristic presence of the regular spherical pores (diameters 14 -15 nm) and ordered hexagonal grid of carbon rods (diameters of 9 and 20 nm) for 3DOMM and CMK-3, respectively.

3.1.2. XRD Analysis

The degree of stacking of graphene layers and their distance in layered carbon materials, 3D organization of the graphene monolayer in regular 3D nanostructured carbon materials, and disorder in amorphous carbon materials were analysed using X-ray powder diffraction. The XRD patterns of graphite, GNPs 2LG, and graphene as typical materials representing well-ordered carbon materials with different numbers of planar graphene layers are shown in Figure 3a. The graphite, 2LG and GNPs patterns show typical graphite lines at 2θ = 23.9°, 26.5°, 42.4°, 44.5°, 54.5°, and 86.8° (PDF file 00-041-1487) characteristic of the layered materials. Graphite exhibits a much larger intensity of diffraction at 26.5 °, corresponding to the layer-to-layer structure of graphite [22, 23, 41] and indicating a larger content of atomic planes with uniform spacing in graphite, compared to GNPs and 2LG. Graphene exhibits the absence of the diffraction line at 26.5°, characteristic of the uniform graphene layering, and the presence of broad signals at around at 25° and 43°, implying that the graphene sheets can be randomly distributed in a corrugated structure. The XRD patterns of the oxidised carbon materials are depicted in Figure 3b. The XRD pattern of Ox-GNPs is characterised by the line at 26.5°, corresponding to the uniform layering of graphene with the same distance between graphene layers as in graphite, and indicating that the layers are not intercalated with oxygen atoms, but

oxygen-containing functional groups may be bound to the edges of the material [23]. The same spacing of the carbon layers of 0.32 nm for graphite, GNPs and Ox-GNPs is consistent with the microscopic measurement. The GtO XRD pattern is characterised by a typical line (002) shifted downward to 11.2° indicating a much larger distance between the graphene layers compared to graphite, as a result of oxygen groups intercalated in the space between the layers and bound to the planar surface of the graphite between the layers [22, 23, 42]. The broad band of Ox-2LG and Ox-SWNTs, centred at approximately 23°, is characteristic of amorphous carbon [14, 41]. The additional band of Ox-SWNTs at 15° [4] corresponds to randomly oriented nanotubes of low crystal order. Figure 3c depicts the XRD patterns of carbon allotropes formed by a 3D organized graphene monolayer. The *Y*-carbon diffractogram comprises a sharp peak at 6.3°, showing that the framework ordering of the FAU was replicated by carbon atoms during the synthesis. This peak corresponds to the (111) planes of the FAU structure retained in the *Y*-carbon replica [21]. Crystalline fullerene C_{60} has typical intense and sharp diffraction responses at 10.9° (111), 17.7° (220), 20.8° (311), 21.8° (222), 27.5° (331), 28.2° (420), 30.9° (422) and 32.9° (511) (PDF file 00-044-0558). The three major peaks correspond to the reflections of planes (111), (220), and (311). Fullerene C_{70} does not exhibit such sharp peaks because of mixing of two structures (fcc and hcp: 9.7° (100), 10.5° (002), 11.0° (101), 14.3° (102), 16.8° (110), 18.5° (103), 19.4° (200), 19.8° (112), 20.11° (201), 21.1° (004) and 27.1° (114)) [17, 43], which confirms the lack of symmetry and therefore orientation disorder [44]. The diffraction lines in Figure 3d confirm the amorphous character of the samples of activated carbons and the 3D organized mesoporous carbons by two broad bands at 2θ = 26.6° and 44.5° that are present in both the AC1 and AC2, and 3DOMM and CMK-3 samples [22, 23, 41]. Asymmetric reflections at 26.5° and 44.5° indicate traces of a turbostratic carbon phase created by the partially parallel oriented carbon layers [45] in the 3D structured 3DOMM and CMK-3. The 3D spatial organization of the mesoporous structure characteristic of 3DOMM and CMK-3 was confirmed using the small-angle X-ray scattering (SAXS) method in our previous studies [32, 34].

3.1.3. Sorption of nitrogen

The nitrogen adsorption-desorption isotherms at 77 K for the series of carbon materials are shown in Figure 4 and obtained values of the surface area and the pore volumes are listed in Table 1. The layered carbon materials (GNPs and graphite) in Figure 4a exhibit Type II isotherms because of unrestricted adsorption on the nonporous materials. For graphene, adsorption at low pressures in the micropores and at higher pressures on the graphene surface

and in the mesopores corresponds to the random folding of crumpled graphene sheets causing the formation of the apparent porosity of the material. The specific surface increases with a decrease in the number of stacked graphene layers. However, it should be considered that layered graphene materials are easily agglomerated as a result of van der Waals cohesive forces [46]. Agglomeration and partial stacking and corrugation of layered graphene materials block a significant part of the surface of graphene sheets in powdered samples [47]. For this reason, in the sorption measurements, nitrogen molecules are adsorbed only on the surface sites available for this molecule and not on the entire surface of the material. The obtained values of the surface area thus only provide information about the surface of the material available under the given measuring conditions for nitrogen molecules, but do not reflect the total surface of layered carbon materials.

The N_2 adsorption on Ox-SWNTs is a composite of Types I and IV isotherms (Figure 4b). The adsorption at low pressures is associated with filling of the tubular micropores in nanotubes and is consistent with HR-TEM analysis indicating a diameter of the nanotubes of about 0.8 – 1.7 nm (Figure 2). Adsorption at higher pressures can be associated with mesopores formed by the nanotubes agglomeration. The adsorption isotherms of GtO and Ox-GNPs showed a small volume of adsorbed nitrogen characteristic of the featureless surface structure. Similar to graphene, the obtained values of the surface area do not reflect the total surface of the layered carbon material but only provide information about the surface of the material that is available for nitrogen molecules.

The 3D organized and especially regularly 3D organized materials shown in Figure 4c enable the adsorption of nitrogen molecules on the vast majority of the surface and the obtained results serve as a reliable estimate of the surface area. The surface area of 2639 $m^2\ g^{-1}$ for zeolite-templated *Y*-carbon formed by 3D graphene curved along the surfaces of the zeolite pore walls corresponds well to the theoretical surface area for graphene of ~2630 $m^2\ g^{-1}$ [47]. The value obtained for a pore volume of 1.56 $cm^3\ g^{-1}$ corresponds to the theoretical pore volume of 1.45 $cm^3\ g^{-1}$ calculated for the replicated channel structure of the faujasite zeolite in the carbon material [48]. Fullerene is an exception to the suitability of surface characterization using nitrogen adsorption among regular 3D materials. The TEM images showed that the spaces between the spherical fullerene C_{60} molecules with a diameter of ~0.7 nm are too small to allow access for nitrogen molecules. Nitrogen sorption thus has only a limited indicative value about the surface area and is not reliably applicable to determining the external surface area of the powdered fullerenes.

The adsorption-desorption isotherms of nitrogen for amorphous and 3D organized amorphous carbon materials are shown in Figure 4d. The isotherms of 3DOMM and CMK-3 correspond to a type IV associated with capillary condensation in the mesopores. The 3DOMM sorption isotherms at higher relative pressure exhibit a hysteresis loop corresponding to type H1 characteristic of uniform cylindrical pores with a mean mesopore diameter of ~14 - 15 nm, in agreement with the TEM analysis (Figure 2). The hysteresis loop for the CMK-3 corresponded to type H2, indicative of cylindrical pores in more complex structures with potential partial restrictions, with a mean mesopore diameter of 3.4 nm. The adsorption isotherms below $P/P_0 = 0.1$ also indicate micropore filling, corresponding to the presence of micropores (Table 1). The sorption data obtained for organized 3D micro-mesoporous materials are characteristic of the structure of 3DOMM and CMK-3 materials [32, 34]. The adsorption-desorption isotherms of nitrogen for both AC samples are quite typical for amorphous carbons with broad pore size distribution. The isotherms indicate adsorption in well-developed micropores with a broader pore size distribution and, to a lesser extent, adsorption in mesopores with a total surface area of 1032 and 895 $m^2 g^{-1}$ for AC1 and AC2, respectively.

3.1.4. XPS Analysis

Analysis of the XPS spectra of the C 1s lines was used to estimate the amount and type of oxygen-containing functional groups present in the series of oxidized carbon materials (Figure 5). The C 1s line with the highest intensity at 284.6 eV, present in the spectra of all the samples, corresponds to carbon atoms without an oxygen ligand. The bands of weaker intensity shifted towards higher binding energies and observed at about 285.8, 286.9, 288.7 and 290.1 eV were assigned to carbon atoms with hydroxyl/phenolic groups (C-OH), C-O-C, ketonic groups (C=O), and carboxyl groups (COOH), respectively [49-53] (see *Supplementary Information*, Table S1). However, the shift in binding energies between the C-OH and C-O-C functional groups is relatively small and assignment based on the binding energy alone is difficult [49, 51]. The assignment was thus confirmed on the basis of analysis of the XPS spectrum of GtO whose structure is characterized by the dominant presence of C-O-C groups. Because the XPS spectrum of GtO (Figure 5b) is characterised by a very intense band at 286.7 eV the band can thus be reliably attributed to C-O-C groups. The abundances of C-O, C-O-C, C=O and O-C=O functional groups and O/C atomic ratio on the surfaces of the samples are listed in Table 2. The concentrations of the oxygen groups indicate a significant degree of oxidation for the Ox-2LG, Ox-GNPs and Ox-SWNTs materials with a predominant

concentration of hydroxyl groups. The XPS spectrum of GtO confirmed the presence of a large number of oxygen-containing groups intercalated in the space between the graphene layers, in agreement with XRD analysis. Photoelectron spectra were also measured for non-oxidized carbon materials (Figure S5); however, the concentrations of oxygen-containing groups were too small (bellow 3%) for their quantitative analysis. The analysis thus confirmed the low level of oxidation of the surface of non-oxidized carbon materials.

3.2 Structure of the Carbon Materials

Structural analysis using a combination of microscopic, diffraction, sorption, and spectroscopic techniques indicated the following structural features of the carbon materials: *Graphene:* The graphene sample is characterised by single atomic carbon layers with wavy and crumpled sheets with lateral size from 0.5 to 5 μm with an admixture of a small amount of 2-5 layered graphene material and a low concentration of oxygen groups on the surface. *Double-layer graphene:* 2LG is formed from two to three graphene layers with a small occurrence of multiple layers and a lateral size of crumpled sheets up to 1 μm. *Graphene nanoplatelets:* GNPs are submicrometer platelets formed from stacked graphene layers with an average of 5 to 20 atomic layers and a low concentration of oxygen groups on the surface. *Graphite:* The graphite sample has the form of fine non-porous particles with particle size of < 50 μm and low external surface area. The sample is characterised by a typical graphite structure with horizontal sheets crystallized in the hexagonal system with high regularity and long-range order and lacking oxygen functional groups. *Oxidised double-layer graphene:* The Ox-2LG sample is characterized by one to several layers of graphene and larger crumpled sheets with populated oxide groups on the surface that contain hydroxyl, ketonic, and carboxyl groups. *Oxidised graphene nanoplatelets:* Ox-GNPs consist of exfoliated graphene nanoplatelets with a typical number of 5-20 layers and highly oxidised edges with a predominant population of hydroxyl groups. *Graphite oxide:* GtO is oxidised powder graphite with the graphite crystal lattice intercalated with oxygen functional groups. The basal planes show a similar arrangement regularity to that of graphite, but the lateral distances between the carbon sheets are expanded from 0.32 to 0.77 nm (the basal XRD peak shifted from 26.5 to 11.3°) by immersion of the oxygen atoms. *Oxidised single-walled nanotubes:* Ox-SWNTs are single-walled nanotubes with typical diameters from 0.8 to 1.7 nm with a small admixture of amorphous material. The surface of the nanotubes is characterized by the presence of oxygen-containing functional groups with a predominance of hydroxyl groups. *Fullerenes:* C_{60} and C_{70} fullerene samples are well-developed non-defective and agglomerated spherical molecules whose walls are formed

from shared pentagonal and hexagonal carbon rings. Fullerene molecules are agglomerated into large units with a regular and tight arrangement. *Zeolite-templated carbon: Y*-carbon is composed of sp^2-hybridized carbon atoms in the deformed graphene layers with shared pentagonal and hexagonal carbon rings with a spatial arrangement that resembles the structure of an inverse replica of the channel system of the faujasite zeolite used as a hard template for material synthesis. The surface area is similar to the theoretical surface area for graphene. The deformed graphene layers contain defects in the form of vacancies. *Activated carbons:* AC samples are micro-mesoporous carbon materials with a well-developed porous structure and a surface of 1032 and 895 $m^2\ g^{-1}$ for AC1 and AC2, respectively. The structure of the activated carbons is composed of graphitic plates with amorphous character and traces of the turbostratic carbon phase created by the partially parallel-oriented carbon layers. *3D organised micro-mesoporous carbon:* 3DOMM is micro-mesoporous amorphous carbon with a 3D ordered spherical mesoporous structure with regular periodicity and interconnection and a large pore volume. The structure was created by faithful replication of the inverse porous structure of the packed monodisperse nanospheres of SiO_2 as a hard template. The regular scaffold that forms the walls of the mesopores is built from microporous amorphous and turbostratic carbon. *CMK-3:* The carbon material CMK-3, prepared by infiltration of a carbon precursor into the SBA-15 silica, used as a hard template, is characterised by an ordered structure that retains the inverse meso-structural order of the SBA-15 silica template. The CMK-3 material is composed of a two-dimensional hexagonal array of carbon rods ~9 and ~20 nm in diameter with interstitial mesopores with mean inner diameter of ~3.4 nm. The carbon rods are formed by amorphous carbon and turbostratic carbon with non-restricted micropores with a pore diameter modus of 1.30 nm.

3.3 Analysis of the Stability of Carbon Materials Using DSC and TG Analysis

It should be noted that the study analysed commonly available carbon materials, which naturally have a certain content of defects and impurities. Thus, the stability cannot be linked exclusively to the theoretical structure of nanostructured carbon materials. The results of thermal analysis show the stability of carbon materials of common and characteristic samples typical for the given types of materials illustrated in Figure 1.

3.3.1 Stability of Carbon-layered Materials

Figure 6a shows the TG/DTG and DSC profiles for materials that differ in the number of layers, from a single layer in graphene to several layers in 2LG, 5-20 layers in GNPs, and a

large number of well-organized graphene layers in graphite. DSC profiles for all layered carbon materials are characterized by asymmetric peaks with maxima at 570, 671, 782 and 894 °C for graphene, 2LG, GNPs and graphite, respectively, summarized in Table 1. The onset and end of all DSC profiles are identical to the beginning and end of the TG curves. It is necessary to note that the analysis of non-defective graphene on the substrate is not possible using the employed thermal analytical methods [30, 54] and therefore we used commercially available graphene in sufficient amounts in the form of freestanding sheets, which contains some defects. However, the onset and end of graphene oxidation deduced from the DSC signal at temperatures of 529 and 575 °C are consistent with the results of a spectroscopic analysis of monolayer graphene oxidation on a support published by Nan et al. [27], which showed that graphene becomes unstable at temperatures from 520 - 560 °C and oxidation is completed at a temperature of 580 °C. A narrower and sharper peak in the DSC profile for graphene compared to multilayer materials shows that graphene was oxidized in a significantly narrower temperature interval. Nan et al. showed by spectroscopic analysis [27] that carbon atoms in graphene first react with oxygen to form sp^3 defects, carbon bond deformation, and vacancy-like defects. The formation of defects in the graphene layer, which is accessible to oxygen from both sides, leads to its very rapid complete oxidation, observed in the DSC profile as a sharp narrow signal. Compared to graphene, the TG/DTG and DSC profiles exhibit an increase in the temperature of the onset of oxidation by 28, 42 and 267 °C, and an increase in the maximum of the DSC profiles by 101, 212 and 324 °C for 2LG, GNPs and graphite, respectively (Figures 6a and 7, Table 1). The very different temperatures for the oxidation of the layered carbon materials indicate how important the stacking of graphene layers is for the stability of carbon materials in the oxidizing environment. Schröder et al. [55] showed that etching a graphene layer with molecular oxygen starts at the edges and vacancies that are accessible to oxygen only on the outer surface of layered carbon materials. Their concentration decreases significantly with increasing numbers of layers. Moreover, Nan et al. [27] suggested that the interaction between graphene layers due to van der Waals forces increases the energy barrier of the upper graphene layer and it is therefore not easily oxidized. The van der Walls forces between two carbon atoms are small compared to the strength of the chemical carbon – carbon bond; however, due to the large number of neighbouring carbon atoms in the layered system, dispersion forces can play a significant role in the stabilization. This was evidenced by spectroscopic studies, which showed that defects do not appear on the graphite surface up to relatively high temperatures [27]. The increasing stability of layered carbon materials with an increasing number of graphene layers is thus a result of the interplay of stabilization of the

carbon layers through van der Waals forces and by the fact that the stacking of graphene layers fundamentally reduces the specific surface available for oxygen and at the same time reduces the number of edges and defective groups, which are primarily associated with the surface of the material.

Large differences in the stability of planar carbon materials differing in the number of layers lead to the question of whether the number of layers is also important in imparting thermal stability of the tubular structures. The TG/DTG-DSC curves obtained for double-walled (DWNTs) and multi-walled carbon nanotubes (MWNTs) showed an increase in characteristic T_{on} from XXX to XXX °C and T_{max} from XXX to XXX °C for DWNTs compared to MWNTs (Figure S6). However, it must be emphasized that the stability of the carbon nanotubes can be also affected by the traces of the metal catalyst used for their synthesis [13, 29], the amount of oxygen groups formed during the purification of the prepared carbon nanotubes from the catalyst, and the amount of amorphous material that is always present in a certain amount in carbon nanotube materials [56].

3.3.2 Stability of Oxidized Carbon Materials

Figure 6b shows the DSC and TG curves obtained for carbon materials containing significant amounts of oxygen-containing functional groups (Ox-2LG, Ox-SWNTs, Ox-GNPs, and GtO). It is obvious that the presence of oxygen groups in carbon materials fundamentally changes their stability in the air. The DSC and TG curves showed decrease in characteristic T_{on} from 557 to 508 °C and a decrease in T_{max} from 671 to 613 °C for 2LG compared to Ox-2LG (Table 1 and Figure 7). The energy barrier for oxidation of the graphene surface containing oxygen functional groups is lower than that of the carbon graphene layer, and the presence of oxygen-containing groups fundamentally reduces the thermal stability. Although the presence of oxygen groups on the surface of two-layered graphene reduces its stability by about 50 °C, the presence of oxygen in GtO causes much greater changes in the thermal stability of graphite. During the oxidation of GtO, the first exothermic peak in DSC already appears at 169 °C and TG shows a decrease in weight at the corresponding temperature. It is known that GtO is already unstable when heated at temperatures of about 150 °C and its thermal decomposition yields large volumes of gaseous products, is exothermic, and, in a large amount, can lead to a thermal runaway reaction [35, 36]. The formation and reaction of the oxygen-containing groups that are present are primarily responsible for the low temperature energetic behaviour [36]. The initiation of a self-propagating thermal deoxygenating reaction of GtO was also described during heating in a nitrogen atmosphere without the presence of oxygen [24, 36]. A second

exothermic peak in the DSC profile of GtO appears at T_{max} 536 °C and corresponds to the oxidation of the remaining carbon material.

The temperatures of the Ox-SWNTs oxidation onset (T_{on} 453 °C) and maximum (T_{max} 543 °C) are even lower than those of Ox-2LG. The necessity of chemical purification of nanotubes after synthesis to remove the metal catalyst used for their synthesis leads to a large number of defects and oxygen-containing groups on their surface. The nanotube preparation methods do not yield pure nanotube products; a certain amount of amorphous carbon and typically multishell sp^2 carbon covering metal catalyst residues is always present in small amounts [13, 29]. In addition to the enrolled cylindrical graphitic sheets forming the nanotubes, HR-TEM and XRD analysis of our nanotube sample detected the presence of poorly defined carbon impurities. Thus, the oxidation of the nanotube sample observed by the TG/DTG and DSC methods cannot be exclusively correlated only with the reactivity of the enrolled cylindrical graphitic sheets but can also be affected by the catalytic properties of the transition metal catalyst residues, with the potential to activate molecular oxygen. Furthermore, the oxidation of the amorphous carbon present in the nanotube sample, which has been shown to be oxidized in activated carbon at about T_{on} 530 °C, can also affect the stability of the of carbon nanotube sample [56]. The thermal stability of the nanotubes is thus given by the interplay of the stability of the single-layer graphite layer itself and the presence of both oxygen related functional groups and transition metal impurities. Complex multistep methods to purify carbon nanotubes lead to a reduction in impurity content to the level of percentage units [29], which, however, may still be a sufficient amount for their catalytic function. The residual mass of the nanotubes after the TG measurement indicates the presence of the remaining amount of metal nanoparticles used in the synthesis of the nanotubes. The thermal analyses results accurately show the thermal stability of the particular sample of oxidised carbon nanotubes; however, they do not provide general information on the stability of the oxidised single-layer carbon cylindrical sheets forming the nanotubes. Effective purification of nanotubes without excessive defect formation can increase their thermal stability [57]; in contrast, the presence of defects arising from the synthesis conditions significantly reduces their thermal stability [15].

Comparison of the characteristic temperatures T_{on} 410 °C and 571 °C for Ox-GNPs and GNPs, respectively, further confirms the great influence of the presence of oxygen functional groups on the thermal stability. Ox-GNPs are characterized by the presence of hydroxyl groups on the edges of the nanosheets. The much lower values of T_{max} and T_{on} for Ox-GNPs compared to GNPs further show that the presence of oxidized edges significantly reduces the overall stability of the material and the initiation of oxidation at the oxidized edges leads to the overall

oxidation of the material at much lower temperatures compared to the non-oxidized carbon material.

3.3.3 Stability of Carbon Allotropes Formed by a 3D Organized Graphene Monolayer

Figure 6c compares the TG/DTG and DSC profiles for materials predominantly formed by a 3D organized single graphene layer (fullerene C_{60}, fullerene C_{70} and *Y*-carbon). The TG/DTG analysis shows that C_{60} fullerene starts to lose weight at 497 °C and the process is complete at 683 °C (Table 1 and Figure 7). This is in excellent agreement with the results of Milliken et al. [16], who found the beginning of weight loss at ~480 °C and the end at ~650 °C. In contrast, Pang et al. observed a maximum temperature of 420 °C for fullerene C_{60} oxidation [11]. Sublimation of fullerene under similar measurement conditions occurs at temperatures above 700 °C [20] and therefore does not contribute to the weight loss observed during the TG analysis; thus the observed loss is associated with the oxidation of the material. Although fullerene, because of its spherical molecular structure, does not contain edges and its structure is virtually defect-free, its thermal stability is not greater compared to graphene (Figure 6a) and *Y*-carbon and many other carbon nanomaterials (see below). The hybridized carbon atoms of sp^2 in the fullerene carbon layer are not within the energy minimum found in planar graphene and the angular strain present in the spherical molecule could affect the stability [58]. Interestingly, the TG profile of fullerene, alone among other material studied, exhibits a slight increase in weight of about 2 w.% during oxidation in the 200-430 °C temperature range before rapid weight loss at higher temperatures. This indicates the accumulation of oxygen groups on the fullerene surface during oxidation at low temperatures. Gallagher and Zhong [19] suggested that the formation of a relatively stable fullerene epoxide (C_{60}-O) [18] may be responsible for the increase in weight. Ismail and Rodgers [20] have shown that C_{60} can chemisorb up to 1.5 oxygen atoms/C_{60} molecule during heating in the air. Subsequent rapid oxidation at higher temperatures is consistent with the low stability of higher fullerene oxides and ozonides [59]. A small amount of oxygen bound to the C_{60} molecule is associated with the development of small heat that is not detectable by DSC. Similar behaviour can also be observed for fullerene C_{70}, where again a small increase in weight is evident in the interval 200-420 °C, but slightly lower temperatures T_{on} 485 °C and T_{max} 601 °C were observed. The lower stability can be caused by the orientational disordered structure of the C_{70} fullerene due to the presence of two different structures [44].

Y-carbon began to lose weight at 496 °C with complete weight loss at 707 °C. The *Y*-carbon is built systematically from a single carbon layer 3D organized along the curved

surfaces of the zeolite pore walls with the same number of imperfections. The structure is assembled of single, non-stacked graphene layers curved as buckybowls that resemble a cross-linked fullerene-like structure. Although *Y*-carbon is characterised by an imperfect structure with populated graphene edges, its stability is similar to that of fullerene without the edges of graphene sheets. The channel structure of the Y zeolite, which determines the spatial arrangement of the carbon replica, is composed of wide supercages and narrower 12-membered ring connections. This can lead to the formation of a graphene layer with sharper or less bent regions, leading to different stresses in a structure with different stability. The stability can then be influenced by the defectiveness of the material, and parts of the material with more or less populated edges can be oxidized more easily. This corresponds to the observation of two maxima during the oxidation of *Y*-carbon in the TG and DSC profiles with maxima at approximately 587 °C and 668 °C (Figure 6c). Kim et al. [48] recently explained the presence of two regions of oxidation by the presence of a more or less defective structure in zeolite-templated carbon materials prepared by different processes that yield more or less defective structures.

3.3.4 Stability of Amorphous Carbon and 3D Organized Mesoporous Carbons

Figure 6d shows a comparison of TG/DTG and DSC profiles for amorphous carbon materials (AC1 and AC2) and a 3D organized mesoporous carbon materials (CMK-3 and 3DOMM). TG/DTG and DSC profiles show that all the materials oxidize at very similar temperatures, regardless of whether the amorphous structure of the material is regularly 3D organized into a mesoporous structure. The maximum temperature of activated carbon oxidation reported at approximately 530 °C [60, 61] is very similar to the T_{on} 537 °C and 527 °C values observed for AC1 and AC2, respectively (Table 1 and Figure 7). The values of T_{on} ∼530 °C and T_{max} ∼620 °C for the amorphous forms of carbon materials are in the range of temperatures required for the oxidation of graphene and 2LG (Table 1). Theoretical studies [62] showed that dissociative chemisorption of molecular oxygen is thermodynamically favourable even on the bare carbon surface; however, the reaction rate of oxidation of the defective carbon structure was observed to be higher and controls the overall stability [26]. The amorphous structure of activated carbon and 3D mesoporous carbon materials, which consist of an amorphous form of carbon, are characterized by the presence of various defects and edges. The presence of populated edges is also characteristic of graphene and 2LG. Since the oxidation of carbon materials starts preferentially at the edges, the thermal stabilities of

graphene, 2LG, activated carbon and 3D mesoporous carbon materials in the air are comparable.

3.3.5 Analysis of Stability of Multiple Brands of the Same Carbon Material

The properties of commercially available carbon nanomaterials often differ depending on the method of their preparation. Nanoscopic properties may differ even if the same processing protocol is followed in different batches. To confirm that the stability of carbon materials is mainly controlled by the characteristic structural features of the given material we analysed the stability of samples of GNPs and activated carbon materials from different producers. GNPs and activated carbon represent materials whose textural properties can vary greatly depending on the method of preparation [63, 64]. The TG/DTG-DSC curves obtained for GNPs and activated carbon materials manufactured by different producers are compared in figure S7. The close T_{on} values of 537, 527 and XXX °C for the three activated carbon samples AC1, AC2 and AC3, respectively, indicate that the stability of the activated carbon is not significantly affected by its origin. Close values of T_{on} 571 and XXX °C were also found for GNPs materials from different manufacturers. We also analysed the temperature stability of zeolite templated carbons from different batches (Figure S8). The course of the TG and DSC curves and the determined values of T_{on}, T_{max} and T_{off} were practically the same for both samples within the measurement error.

3.4 Relationships between Structure and Stability of Carbon Materials

3.4.1 The Effect of Stacking of Graphene Layers on the Stability of Carbon-layered Materials

The onset (T_{on}) and maximum (T_{max}) oxidation temperatures for the studied carbon materials observed in a wide range of temperatures from 169 to 796 °C and from 197 to 894 °C, respectively, show that the structure of carbon materials greatly affects their stability in the air (Table 1 and Figure 7). The increase in the number of layers from one to two resulted in an increase in T_{max} by 100 °C, for 5-20 layers by 210 °C and for a large number of graphite layers by 320 °C (Figure 7). Obviously, the most important parameter increasing the stability among all the studied carbon materials is the stacking of individual graphene layers. The increase in stability is associated with an interplay of parameters including van der Waals forces between graphene layers, stabilizing the outer graphene layer [27], reduction of the outer surface available for oxygen, and reduction of the number of defects on the surface. For single-layer graphene, oxidation takes place very quickly in a narrow temperature interval of 45 °C; the oxidation process extends to higher temperatures with increasing numbers of layers, where the

interval is as wide as 270 °C for multilayer structures. The oxidation rate of carbon materials is influenced by their specific surface area available for oxygen [65] and for multi-layered carbon materials can be influenced by the oxidation kinetics [66].

3.4.2 Effect of 3D organization of graphene monolayer and structure disorder on stability

Cylindrical fullerenes C_{60} and C_{70} composed of a single layer carbon sheet of linked, regularly arranged hexagonal and pentagonal rings forming a non-defective structure, exhibited the onset of oxidation at a temperature slightly lower than that for graphene. Although fullerene contains no edges and its structure is defect-free, its thermal stability is reduced by the angular strains present in the spherical molecule, which has a significantly higher energy compared to planar graphene [58]. Although all the other carbon materials lose weight during oxidation due to the formation of gaseous oxidation products, the unique structure of fullerene enables an extraordinarily selective reaction with gaseous molecular oxygen. The electrophilic addition of oxygen atoms to 6,6-double bonds reduces the angle deformation in the fullerene molecule by changing sp^2-hybridized carbons into sp^3-hybridized ones in the formed fullerene epoxides [58]. The bond angles decrease from ~ 120° in the hybridized sp^2 orbitals to ~ 110° in the sp^3 orbitals [58]. The resulting intermediate is then oxidized at temperatures similar to those for *Y*-carbon. The similarity in the structures of fullerenes and *Y*-carbon, which is built systematically from single carbon layers 3D organised and curved like buckybowls resembling a linked fullerene-like structure with the same degree of imperfections, results in a similar stability in the air.

The group of materials with defective structures, such as activated carbon or mesoporous 3D organized materials, which are characterized by an amorphous structure without regular organization of the graphene layers with edges and possible vacancies, are all oxidized in the temperature range, T_{on} 496 - 537 °C and T_{max} 618 - 668 °C, which are similar to nanomaterials consisting mainly of one graphene layer T_{on} 485 - 529 °C and T_{max} 570 - 621 °C for fullerenes, graphene and *Y*-carbon (Table 1 and Figure 7).

It follows that carbon nanomaterials that are formed by a regularly organized monolayer of graphene stressed by bending (Fullerenes) or contain structural defects (*Y*-carbon) exhibit similar thermal stabilities in the air to porous amorphous carbon materials (activated carbon) and 3D organized mesoporous carbon materials.

3.4.3 Reduced Stability of Oxidized Carbon Materials

A significant decrease in the stability is associated with the presence of oxygen functional groups on the surface of carbon materials, both those formed by a single or few graphene layers (Ox-SWNTs, Ox-2LG) and those formed by stacked graphene layers (Ox-GNPs, GtO). The presence of functional oxygen groups in GtO is associated with a dramatic decrease in stability. Epoxy groups have been associated in the literature [36] with the oxidation of GtO below 200 °C, which is consistent with the observation of a T_{on} of 169 °C for the studied GtO. A significant decrease in stability is also associated with the presence of hydroxyl groups on the surfaces of carbon materials [67]. The T_{on} values of 410 °C and 568 °C for Ox-GNPs and GNPs, respectively, show that stability under the given measurement conditions is reduced by partial oxidation of the surface by 150 °C (Table 1 and Figure 7).

Conclusions

Analysis of the thermal stability of carbon nanomaterials including planar structures with different numbers of graphene layers (graphene, 2LG, GNPs and graphite), oxidized carbon materials (Ox-2LG, Ox-SWNTs, Ox-GNPs and GtO), 3D carbon materials with a single graphene layer (fullerenes C_{60} and C_{70} and *Y*-carbon) and amorphous and 3D organized mesoporous carbon materials (3DOMM and CMK-3) yielded the following parameters that determine the stability of carbon materials:

i) The decisive factor in increasing the stability of carbon materials is the stacking of graphene layers parallel to each other with a long-range order. The stacking of graphene layers fundamentally reduces the specific surface available for oxygen, reduces the number of edges and defective groups associated with the surface, and the interaction between graphene layers enhances the energy barrier for oxidation of the upper graphene layer. The temperature (T_{max}) required for oxidation increased from 570 °C for graphene to 782 °C for nanoscale graphite particles formed of stacked 15 to 20 atomic layers, up to 894 °C for graphite with long-range crystalline order.

ii) The most significant factor for reducing the stability of carbon materials is the presence of specific oxygen-containing functional groups on oxidized carbon materials, lowering the energy barrier for the oxidation of the carbon layer. The functional oxygen groups in graphite oxide resulted in rapid oxidation of the carbon material at a temperature as low as 169 °C. The stability is also significantly reduced by the presence of hydroxyl groups on the surface of oxidized carbon materials. The highly oxidized edges with the prevailing population of hydroxyl groups enabled the oxidation of the graphene

nanoplatelets at a temperature of more than 150 °C lower compared to the material without a significantly increased concentration of oxygen functional groups.

iii) The stability is obviously also affected by the presence of edges and defects; however, analysis has shown that non-defective monolayers in fullerenes, defective monolayers in zeolite-templated carbon, disordered amorphous carbon materials, as well as 3D-organised mesoporous carbon materials exhibit comparable stability and were oxidized within a relatively narrow temperature window with values of T_{on} between 485 and 537 °C.

The stability of carbon materials is thus mainly controlled by the interplay of the stacking of graphene layers and the concentration and nature of defects in the form of mainly oxygen-containing functional groups. The stability of the analysed carbon materials increased in the following order: GtO < Ox-2LG ~ Ox-SWNTs ~ Ox-GNPs < graphene ~ fullerene C_{60} ~ fullerene C_{70} ~ *Y*-carbon ~ activated carbon ~ 3DOMM ~ CMK-3 < GNPs < graphite.

Acknowledgements

This work was supported by the Czech Science Foundation under Project No. 21-07753S. The authors acknowledge the assistance provided by the Research Infrastructure NanoEnviCz (Projects No. LM2018124, CZ.02.1.01/0.0/0.0/16 013/0001821, CZ.02.1.01/0.0/0.0/18 046/0015586), supported by the Ministry of Education, Youth and Sports of the Czech Republic and The European Union - European Structural and Investments Funds in the frame of Operational Programme Research Development and Education.

References

[1] Y. Liang, Y. Li, H. Wang, J. Zhou, J. Wang, T. Regier, H. Dai, Co3O4 nanocrystals on graphene as a synergistic catalyst for oxygen reduction reaction, Nature Materials, 10 (2011) 780-786.
[2] C. Tan, X. Cao, X.J. Wu, Q. He, J. Yang, X. Zhang, J. Chen, W. Zhao, S. Han, G.H. Nam, M. Sindoro, H. Zhang, Recent Advances in Ultrathin Two-Dimensional Nanomaterials, Chemical Reviews, 117 (2017) 6225-6331.
[3] P. Sazama, J. Pastvova, C. Rizescu, A. Tirsoaga, V.I. Parvulescu, H. Garcia, L. Kobera, J. Seidel, J. Rathousky, P. Klein, I. Jirka, J. Moravkova, V. Blechta, Catalytic Properties of 3D Graphene-Like Microporous Carbons Synthesized in a Zeolite Template, ACS Catalysis, 8 (2018) 1779-1789.
[4] J.L. Figueiredo, M.F.R. Pereira, The role of surface chemistry in catalysis with carbons, Catalysis Today, 150 (2010) 2-7.
[5] D.S. Su, N. Maksimova, J.J. Delgado, N. Keller, G. Mestl, M.J. Ledoux, R. Schlogl, Nanocarbons in selective oxidative dehydrogenation reaction, Catalysis Today, 102 (2005) 110-114.
[6] J. Zhang, X. Liu, R. Blume, A.H. Zhang, R. Schlogl, D.S. Su, Surface-modified carbon nanotubes catalyze oxidative dehydrogenation of n-butane, Science, 322 (2008) 73-77.
[7] D.S. Su, R. Schlogl, Nanostructured Carbon and Carbon Nanocomposites for Electrochemical Energy Storage Applications, Chemsuschem, 3 (2010) 136-168.

[8] A. Ghosh, Y.H. Lee, Carbon-Based Electrochemical Capacitors, Chemsuschem, 5 (2012) 480-499.
[9] C.J. Shearer, A. Cherevan, D. Eder, Application and Future Challenges of Functional Nanocarbon Hybrids, Advanced Materials, 26 (2014) 2295-2318.
[10] Polymer nanocomposites, MRS Bulletin, 32 (2007) 314-319.
[11] L.S.K. Pang, J.D. Saxby, S.P. Chatfield, Thermogravimetric analysis of carbon nanotubes and nanoparticles, The Journal of Physical Chemistry, 97 (1993) 6941-6942.
[12] R. Yu, L. Chen, Q. Liu, J. Lin, K.L. Tan, S.C. Ng, H.S.O. Chan, G.Q. Xu, T.S.A. Hor, Platinum Deposition on Carbon Nanotubes via Chemical Modification, Chemistry of Materials, 10 (1998) 718-722.
[13] H. Hu, B. Zhao, M.E. Itkis, R.C. Haddon, Nitric Acid Purification of Single-Walled Carbon Nanotubes, The Journal of Physical Chemistry B, 107 (2003) 13838-13842.
[14] N.I. Kovtyukhova, T.E. Mallouk, L. Pan, E.C. Dickey, Individual single-walled nanotubes and hydrogels made by oxidative exfoliation of carbon nanotube ropes, J Am Chem Soc, 125 (2003) 9761-9769.
[15] L. Chen, X.-j. Pang, Q.-t. Zhang, Z.-l. Yu, Cutting of carbon nanotubes by a two-roller mill, Materials Letters, 60 (2006) 241-244.
[16] J. Milliken, T.M. Keller, A.P. Baronavski, S.W. McElvany, J.H. Callahan, H.H. Nelson, Thermal and oxidative analyses of buckminsterfullerene, C60, Chemistry of Materials, 3 (1991) 386-387.
[17] G.B.M. Vaughan, P.A. Heiney, J.E. Fischer, D.E. Luzzi, D.A. Rickettsfoot, A.R. Mcghie, Y.W. Hui, A.L. Smith, D.E. Cox, W.J. Romanow, B.H. Allen, N. Coustel, J.P. Mccauley, A.B. Smith, Orientational Disorder in Solvent-Free Solid C70, Science, 254 (1991) 1350-1353.
[18] J.M. Wood, B. Kahr, S.H. Hoke, L. Dejarme, R.G. Cooks, D. Ben-Amotz, Oxygen and methylene adducts of C60 and C70, J Am Chem Soc, 113 (1991) 5907-5908.
[19] P.K. Gallagher, Z. Zhong, Some applications of thermal analysis to fullerenes, Journal of thermal analysis, 38 (1992) 2247-2255.
[20] I.M.K. Ismail, S.L. Rodgers, Comparisons between fullerene and forms of well-known carbons, Carbon, 30 (1992) 229-239.
[21] N. Alam, R. Mokaya, Evolution of optimal porosity for improved hydrogen storage in templated zeolite-like carbons, Energ Environ Sci, 3 (2010) 1773-1781.
[22] M.-C. Hsiao, S.-H. Liao, M.-Y. Yen, C.-C. Teng, S.-H. Lee, N.-W. Pu, C.-A. Wang, Y. Sung, M.-D. Ger, C.-C.M. Ma, Preparation and properties of a graphene reinforced nanocomposite conducting plate, Journal of Materials Chemistry, 20 (2010) 8496-8505.
[23] M.C. Hsiao, S.H. Liao, M.Y. Yen, P.I. Liu, N.W. Pu, C.A. Wang, C.C.M. Ma, Preparation of Covalently Functionalized Graphene Using Residual Oxygen-Containing Functional Groups, Acs Appl Mater Inter, 2 (2010) 3092-3099.
[24] F. Kim, J. Luo, R. Cruz-Silva, L.J. Cote, K. Sohn, J. Huang, Self-Propagating Domino-like Reactions in Oxidized Graphite, Advanced Functional Materials, 20 (2010) 2867-2873.
[25] D.C. Marcano, D.V. Kosynkin, J.M. Berlin, A. Sinitskii, Z. Sun, A. Slesarev, L.B. Alemany, W. Lu, J.M. Tour, Improved Synthesis of Graphene Oxide, ACS Nano, 4 (2010) 4806-4814.
[26] C.I. Contescu, T. Guldan, P. Wang, T.D. Burchell, The effect of microstructure on air oxidation resistance of nuclear graphite, Carbon, 50 (2012) 3354-3366.
[27] H.Y. Nan, Z.H. Ni, J. Wang, Z. Zafar, Z.X. Shi, Y.Y. Wang, The thermal stability of graphene in air investigated by Raman spectroscopy, Journal of Raman Spectroscopy, 44 (2013) 1018-1021.
[28] A. Cuesta, M. Jamond, A. Martínez-Alonso, J.M.D. Tascón, Thermal behavior of fullerenes in different gas atmospheres, Carbon, 34 (1996) 1239-1248.
[29] S.R. Vivekchand, R. Jayakanth, A. Govindaraj, C.N. Rao, The problem of purifying single-walled carbon nanotubes, Small, 1 (2005) 920-923.
[30] A.G. Bannov, M.V. Popov, P.B. Kurmashov, Thermal analysis of carbon nanomaterials: advantages and problems of interpretation, Journal of Thermal Analysis and Calorimetry, 142 (2020) 349-370.
[31] J.A. Zapata H, S.L. Simon, B.P. Grady, Influence of diameter on the degradation profile of multiwall carbon nanotubes, Journal of Thermal Analysis and Calorimetry, 138 (2019) 1351-1362.

[32] M. Vorokhta, J. Morávková, M. Dopita, A. Zhigunov, M. Šlouf, R. Pilař, P. Sazama, Effect of micropores on CO2 capture in ordered mesoporous CMK-3 carbon at atmospheric pressure, Adsorption, 27 (2021) 1221-1236.
[33] W. Fan, M.A. Snyder, S. Kumar, P.S. Lee, W.C. Yoo, A.V. McCormick, R. Lee Penn, A. Stein, M. Tsapatsis, Hierarchical nanofabrication of microporous crystals with ordered mesoporosity, Nature Materials, 7 (2008) 984-991.
[34] M. Vorokhta, J. Morávková, D. Řimnáčová, R. Pilař, A. Zhigunov, M. Švábová, P. Sazama, CO2 capture using three-dimensionally ordered micromesoporous carbon, Journal of CO2 Utilization, 31 (2019) 124-134.
[35] D. Krishnan, F. Kim, J. Luo, R. Cruz-Silva, L.J. Cote, H.D. Jang, J. Huang, Energetic graphene oxide: Challenges and opportunities, Nano Today, 7 (2012) 137-152.
[36] Y. Qiu, F. Collin, R.H. Hurt, I. Külaots, Thermochemistry and kinetics of graphite oxide exothermic decomposition for safety in large-scale storage and processing, Carbon, 96 (2016) 20-28.
[37] R.W.M. Kwok, XPSPEAK, version 4.1., Hong Kong, 1999. Available online: http://www.phy.cuhk.edu.hk/surface/XPSPeak, 1999.
[38] J.C. Meyer, A.K. Geim, M.I. Katsnelson, K.S. Novoselov, T.J. Booth, S. Roth, The structure of suspended graphene sheets, Nature, 446 (2007) 60-63.
[39] S. Aghili, M. Panjepour, M. Ghiaci, Degradation mechanism and oxidation kinetics of C60 fullerene, Diamond and Related Materials, 124 (2022) 108943.
[40] P. Toth, Nanostructure quantification of turbostratic carbon by HRTEM image analysis: State of the art, biases, sensitivity and best practices, Carbon, 178 (2021) 688-707.
[41] X.M. Sun, J.F. Liu, Y.D. Li, Oxides@C core-shell nanostructures: One-pot synthesis, rational conversion, and Li storage property, Chemistry of Materials, 18 (2006) 3486-3494.
[42] Y.X. Xu, H. Bai, G.W. Lu, C. Li, G.Q. Shi, Flexible graphene films via the filtration of water-soluble noncovalent functionalized graphene sheets, J Am Chem Soc, 130 (2008) 5856-+.
[43] K. Onishi, K. Sezaimaru, F. Nakashima, Y. Sun, K. Kirimoto, M. Sakaino, S. Kanemitsu, Current-voltage characteristics of C-70 solid near Meyer-Neldel temperature, J Appl Phys, 121 (2017).
[44] S. Sachdeva, D. Singh, S.K. Tripathi, Optical and electrical properties of fullerene C70 for solar cell applications, Opt Mater, 101 (2020).
[45] B. McEnaney, Properties of Activated Carbons, Handbook of Porous Solids2002, pp. 1828-1863.
[46] H.K. Chae, D.Y. Siberio-Pérez, J. Kim, Y. Go, M. Eddaoudi, A.J. Matzger, M. O'Keeffe, O.M. Yaghi, D. Materials, G. Discovery, A route to high surface area, porosity and inclusion of large molecules in crystals, Nature, 427 (2004) 523-527.
[47] F. Bonaccorso, L. Colombo, G. Yu, M. Stoller, V. Tozzini, A.C. Ferrari, R.S. Ruoff, V. Pellegrini, Graphene, related two-dimensional crystals, and hybrid systems for energy conversion and storage, Science, 347 (2015) 1246501.
[48] K. Kim, T. Lee, Y. Kwon, Y. Seo, J. Song, J.K. Park, H. Lee, J.Y. Park, H. Ihee, S.J. Cho, R. Ryoo, Lanthanum-catalysed synthesis of microporous 3D graphene-like carbons in a zeolite template, Nature, 535 (2016) 131-135.
[49] F.T. Johra, J.W. Lee, W.G. Jung, Facile and safe graphene preparation on solution based platform, J Ind Eng Chem, 20 (2014) 2883-2887.
[50] R. Muzyka, S. Drewniak, T. Pustelny, M. Chrubasik, G. Gryglewicz, Characterization of Graphite Oxide and Reduced Graphene Oxide Obtained from Different Graphite Precursors and Oxidized by Different Methods Using Raman Spectroscopy, Materials, 11 (2018) 1050.
[51] S. Park, J.H. An, I.W. Jung, R.D. Piner, S.J. An, X.S. Li, A. Velamakanni, R.S. Ruoff, Colloidal Suspensions of Highly Reduced Graphene Oxide in a Wide Variety of Organic Solvents, Nano Lett, 9 (2009) 1593-1597.
[52] D. Yang, A. Velamakanni, G. Bozoklu, S. Park, M. Stoller, R.D. Piner, S. Stankovich, I. Jung, D.A. Field, C.A. Ventrice, R.S. Ruoff, Chemical analysis of graphene oxide films after heat and chemical treatments by X-ray photoelectron and Micro-Raman spectroscopy, Carbon, 47 (2009) 145-152.

[53] R.B. Yi, X.M. Xia, R.J. Yang, R.S. Yu, F.F. Dai, J.L. Chen, W. Liu, M. Wu, J. Xu, L. Chen, Selective reduction of epoxy groups in graphene oxide membrane for ultrahigh water permeation, Carbon, 172 (2021) 228-235.
[54] P. Rodríguez-Estupiñán, I. Miranda-Carvajal, P.C. Campos, C.A. Guerrero-Fajardo, L. Giraldo, J.C. Moreno-Piraján, Graphene-based materials: analysis through calorimetric techniques, Journal of Thermal Analysis and Calorimetry, 147 (2022) 9301-9351.
[55] U.A. Schröder, E. Grånäs, T. Gerber, M.A. Arman, A.J. Martínez-Galera, K. Schulte, J.N. Andersen, J. Knudsen, T. Michely, Etching of graphene on Ir(111) with molecular oxygen, Carbon, 96 (2016) 320-331.
[56] A.M.F. Lima, A.W. Musumeci, H.-W. Liu, E.R. Waclawik, G.G. Silva, Purity evaluation and influence of carbon nanotube on carbon nanotube/graphite thermal stability, Journal of Thermal Analysis and Calorimetry, 97 (2009) 257.
[57] A.W. Musumeci, G.G. Silva, W.N. Martens, E.R. Waclawik, R.L. Frost, Thermal decomposition and electron microscopy studies of single-walled carbon nanotubes, Journal of Thermal Analysis and Calorimetry, 88 (2007) 885-891.
[58] K.C.V. Lynn, Nanotechnology: Principles and Practices, EDTECH2018.
[59] D. Heymann, R.B. Weisman, Fullerene oxides and ozonides, Comptes Rendus Chimie, 9 (2006) 1107-1116.
[60] E. Illeková, K. Csomorová, Kinetics of oxidation in various forms of carbon, Journal of Thermal Analysis and Calorimetry, 80 (2005) 103-108.
[61] Y. Xiao, K.-H. Liu, P. Pang, C.-M. Shu, Thermokinetics behaviour and parameters for spontaneous combustion of carbonised powders and oxidised powders from preparation of coal-based activated carbon, Journal of Thermal Analysis and Calorimetry, 144 (2021) 415-424.
[62] Z.H. Zhu, J. Finnerty, G.Q. Lu, R.T. Yang, A Comparative Study of Carbon Gasification with O2 and CO2 by Density Functional Theory Calculations, Energy & Fuels, 16 (2002) 1359-1368.
[63] A. Ahmadpour, D.D. Do, The preparation of activated carbon from macadamia nutshell by chemical activation, Carbon, 35 (1997) 1723-1732.
[64] Q.T. Truong, P. Pokharel, G.S. Song, D.S. Lee, Preparation and characterization of graphene nanoplatelets from natural graphite via intercalation and exfoliation with tetraalkylammoniumbromide, Journal of Nanoscience and Nanotechnology, 2012, pp. 4305-4308.
[65] W. Jiang, G. Nadeau, K. Zaghib, K. Kinoshita, Thermal analysis of the oxidation of natural graphite — effect of particle size, Thermochimica Acta, 351 (2000) 85-93.
[66] K. Zaghib, X. Song, K. Kinoshita, Thermal analysis of the oxidation of natural graphite: isothermal kinetic studies, Thermochimica Acta, 371 (2001) 57-64.
[67] J.F. Espinal, F. Mondragón, T.N. Truong, Thermodynamic evaluation of steam gasification mechanisms of carbonaceous materials, Carbon, 47 (2009) 3010-3018.

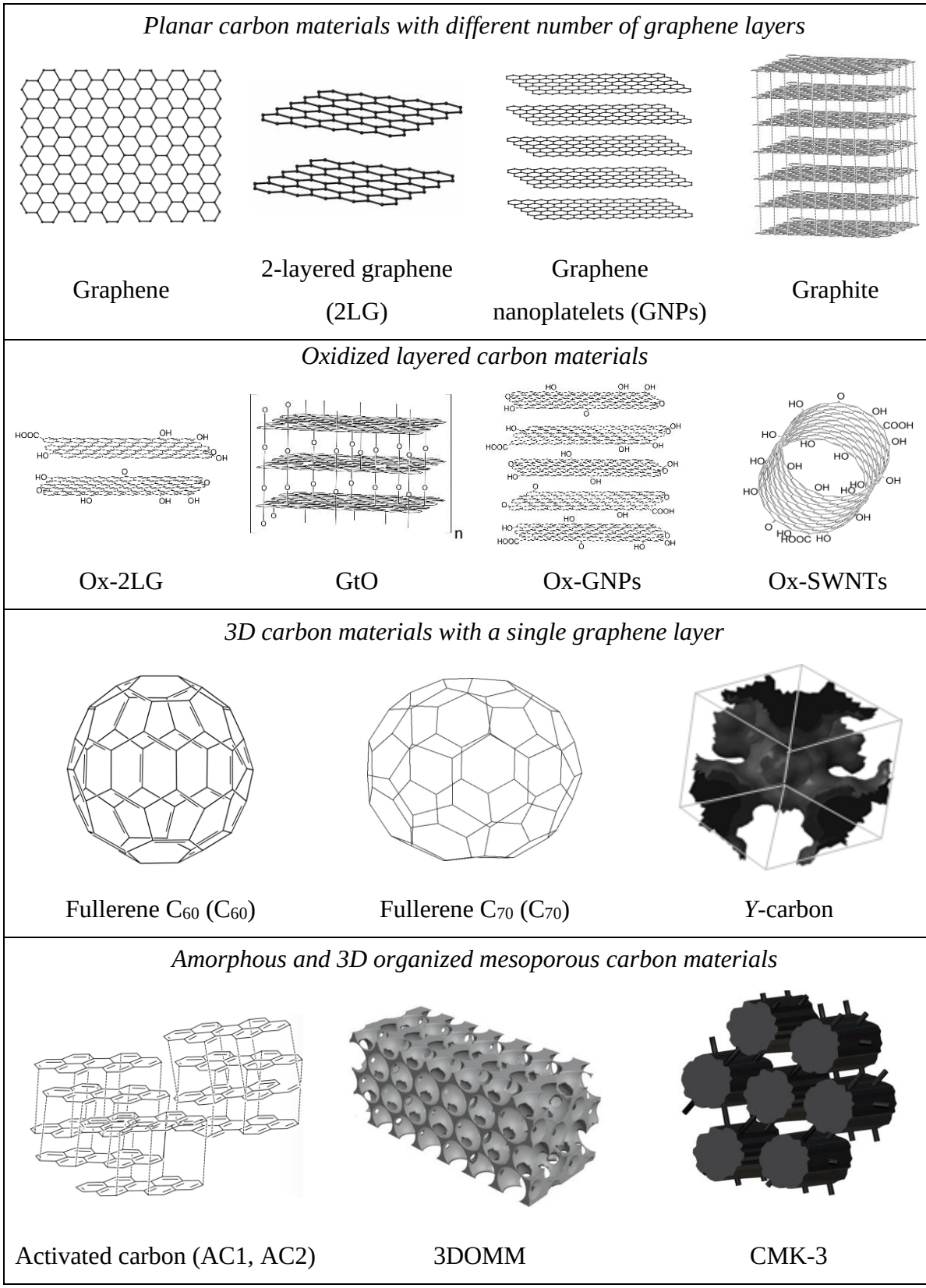

Figure 1. Illustration of the structure of studied carbon materials.

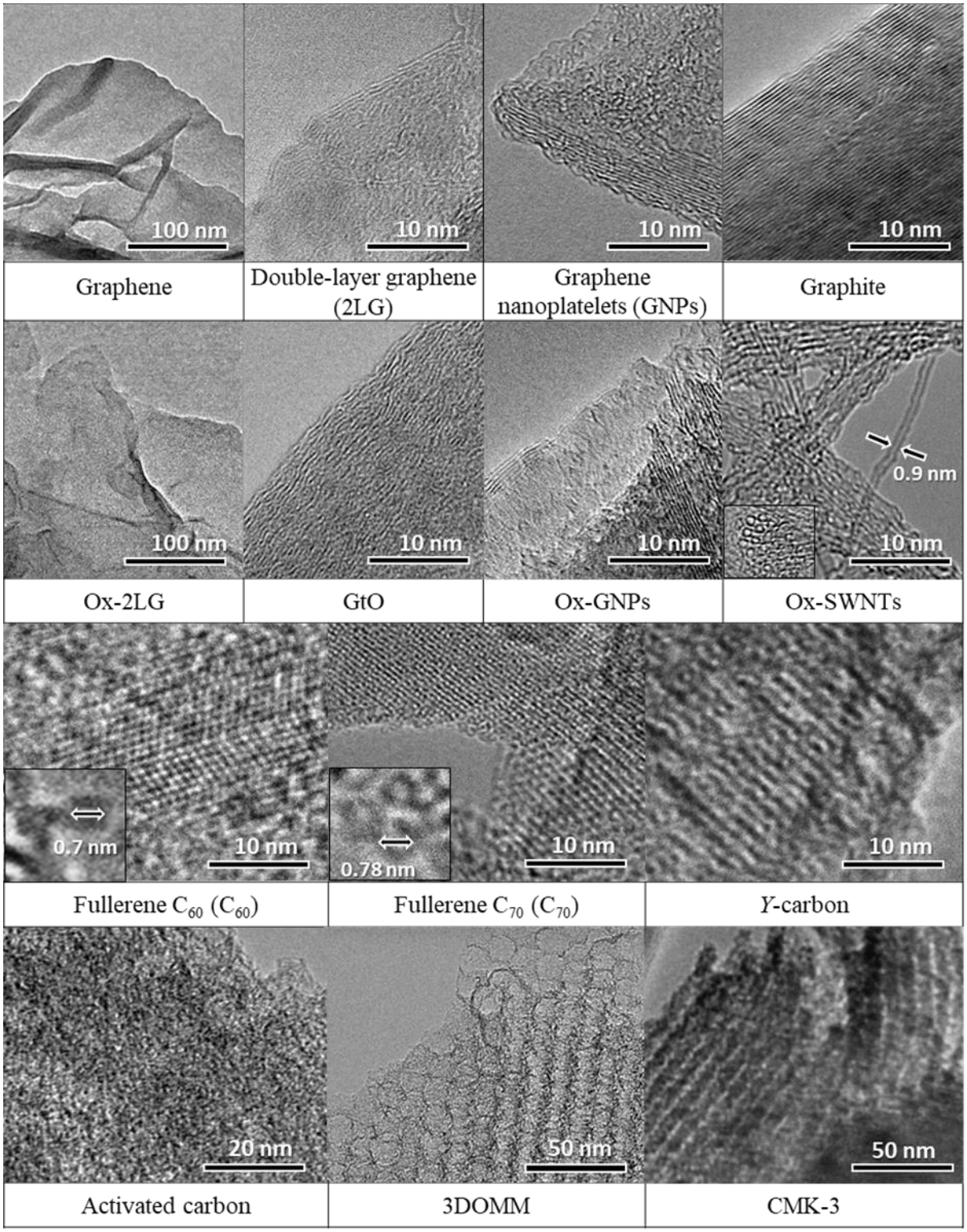

Figure 2. Representative high-resolution transmission electron microscopy images of studied carbon materials.

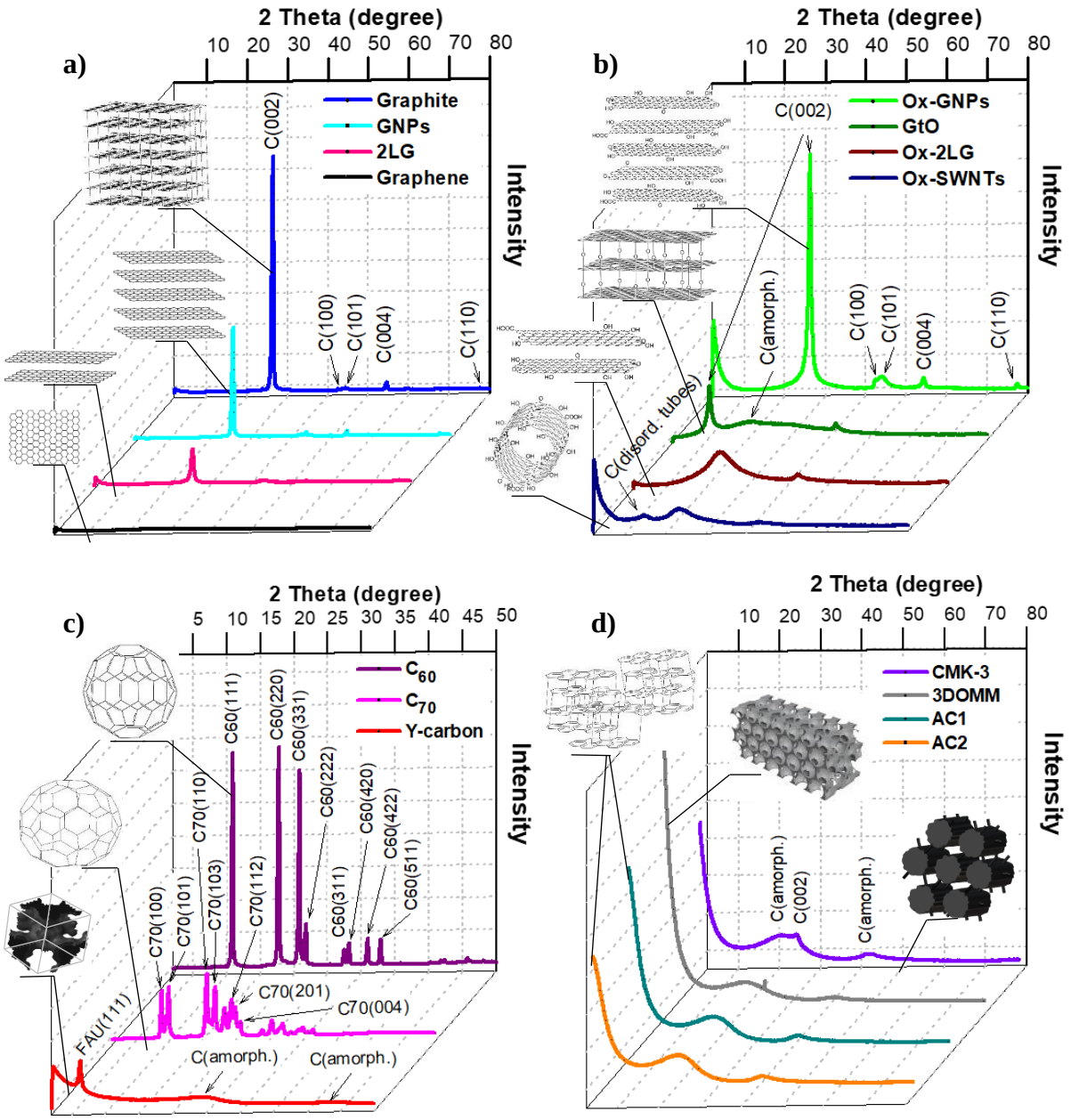

Figure 3. X-ray diffractograms of a) planar carbon materials with different number of graphene layers, b) oxidized carbon materials, c) 3D carbon materials with a single graphene layer, and d) amorphous 3D organised mesoporous and activated carbon materials.

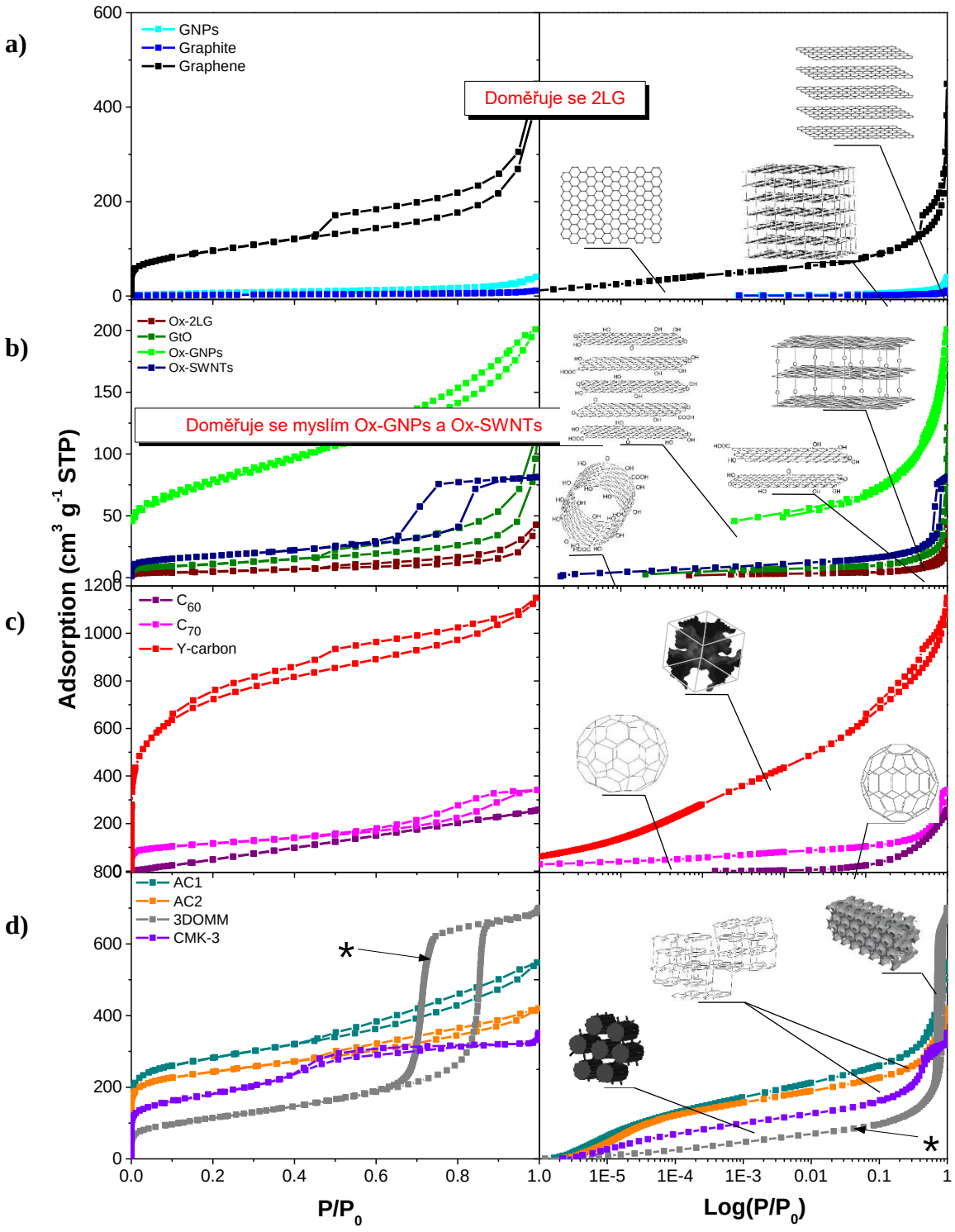

Figure 4. N_2 adsorption/desorption at 77 K for a) planar carbon materials with different number of graphene layers, b) oxidized layered carbon materials, c) 3D carbon materials with a single graphene layer, and d) amorphous 3D organised mesoporous and activated carbon materials. *-multiplied by 0.3 for better resolution of the remaining curves.

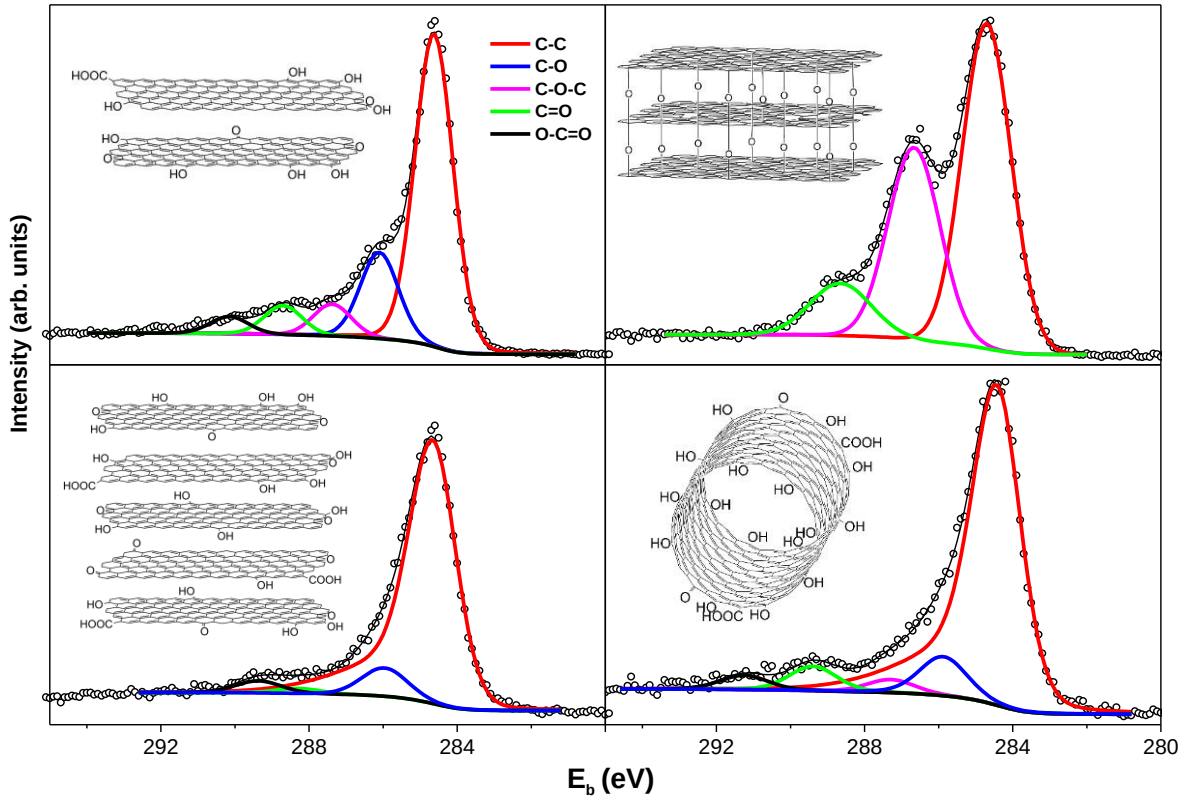

Figure 5. Analysis of the XPS spectra of the C 1s line for the oxidized carbon materials. a) Ox-2LG, b) GtO, c) Ox-GNPs, and d) Ox-SWNTs.

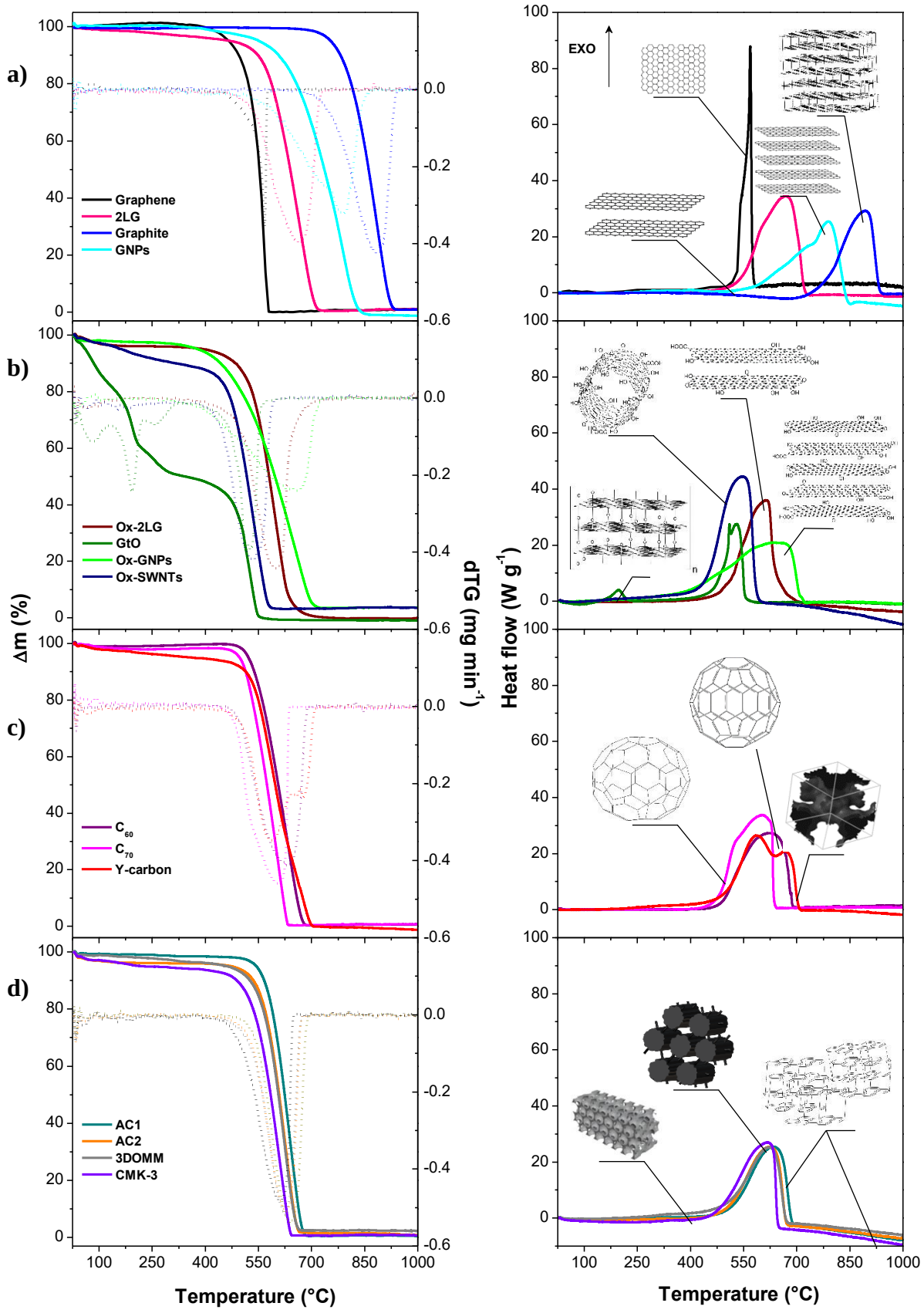

Figure 6. TG/DTG-DSC analysis of thermal stability of a) planar single- and multi-layered carbon materials, b) oxidized carbon materials, c) 3D carbon materials with a

single layer of graphene, and d) and amorphous 3D organised mesoporous carbon and activated carbon materials in air.

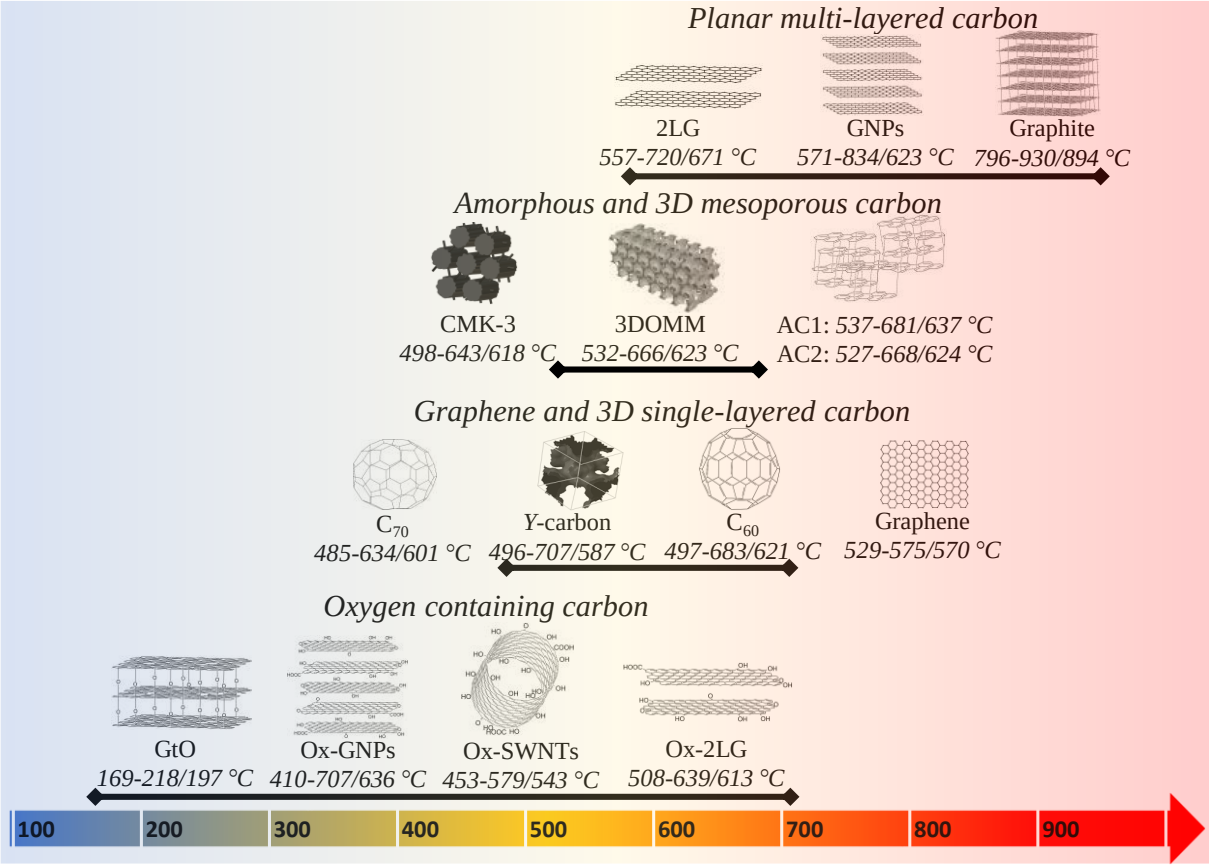

Figure 7. Thermal stability of nanostructured carbon materials in air. The onset (T_{on}), maximum (T_{max}) and offset (T_{off}) temperatures are indicated (e.g. 169-218/197 °C for GtO means T_{on} 169 °C, T_{off} 218 °C and T_{max} 197 °C).

Table 1. Textural characteristics and DSC analysis of the thermal stability of carbon materials in air with the characteristic onset (T_{on}), maximum (T_{max}) and the offset (T_{off}) temperatures determined from the DSC signals.

Sample (Abbreviation)	V_{micro} cm^3 g^{-1}	V_{meso} cm^3 g^{-1}	S_{tot} m^2 g^{-1}	V_{tot} cm^3 g^{-1}	T_{on} °C	T_{max} °C	T_{off} °C
Planar carbon materials with different number of graphene layers							
Graphene, single layer (G)	0.01	0.08	342	0.09	529±3	570±1	575±1
Graphene, 2-3 layers (2LG)	-	-	-	-	557±1	671±2	720±1

Graphene nanoplatelets, 15-20 layers (GNPs)	0.01	-	26	-	571±2	782±5	834±2
Graphite	-	-	8	-	796±5	894±4	930±3
Oxidized layered carbon materials							
Oxidized 2-3 layered graphene (Ox-2LG)	0	<0.01	18	<0.01	508±2	613±4	639±3
Graphite oxide (GtO)	0	0.01	40	0.01	169±1	197±1	218±1
					460±5	536±4	553±1
Oxidized graphene nanoplatelets (Ox-GNPs)	0.01	0.30	277	0.31	410±1	636±8	707±1
Oxidized single-walled nanotubes (Ox-SWNTs)					453±3	543±3	579±2
3D carbon materials with a single graphene layer							
Fullerene C60 (C60)	n.d.[c]	n.d.[c]	n.d.[c]	n.d.[c]	497±4	621±3	683±3
Fullerene C70 (C70)	0.06	0.07	412	0.13	485±1	601±1	634±1
Y-zeolite-templated carbon (*Y*-carbon)	0.73	0.83	2639	1.56	496±5	587±1	707±2
						668±2	
Amorphous and 3D organized mesoporous carbon materials							
Activated carbon (AC1)	0.21	0.21	1032	0.42	537±1	637±2	681±1
Activated carbon (AC2)	0.37	0.20	895	0.57	527±1	624±1	668±1
3-dimensional ordered macro-mesoporous carbon (3DOMM)	0.17	3.42	1343	3.59	532±3	623±1	666±1
Ordered mesoporous carbon nanomaterial (CMK-3)	0.03	0.37	624	0.40	498±1	618±1	643±1

[a] *Analysed by N_2 adsorption at 77 K and BdB t-plot method*

[b] $V_{meso} = V_{total} - V_{micro}$

[c] *Not determined due to the agglomeration of fullerene particles*

Table 2. Distribution of functional groups of C-OH, C-O-C, C=O, and O-C=O (at. %) in the oxidized carbon samples.

Sample (Abbreviation)	**C-OH** **at. %**	**C-O-C** **at. %**	**C=O** **at. %**	**O-C=O** **at. %**
Oxidized 2-3 layered graphene (Ox-2LG)	9.7	4.7	4.1	2.2
Graphite oxide (GtO)	0.0	34.0	9.7	0.0
Oxidized graphene nanoplatelets (Ox-GNPs)	6.9	1.3	3.0	0.0
Oxidized single-walled nanotubes (Ox-SWNTs)	7.4	2.5	4.6	2.7

Supplementary information

Thermal Stability of Nanostructured Carbon Materials in Air

Galina Sádovská[1,2], Pavla Honcová[2], Jaroslava Morávková[1], Ivan Jirka[1], Maryna Vorokhta[3], Radim Pilař[1], Jiří Rathouský[1], Dalibor Kaucký[1], Martin Mergl[1], Petr Sazama[1*]

[1]J. Heyrovsky Institute of Physical Chemistry, Academy of Sciences of the Czech Republic, Dolejskova 2155/3, 182 23 Prague, Czech Republic, [*]Corresponding author: petr.sazama@jh-inst.cas.cz

[2]Institute of Organic Chemistry and Technology, Faculty of Chemical Technology, University of Pardubice, Studentska 573, 532 10 Pardubice, Czech Republic

[3]Department of Geochemistry, Institute of Rock Structure and Mechanics, Czech Academy of Sciences, V Holesovickach 94/41, 18209 Prague 8, Czech Republic

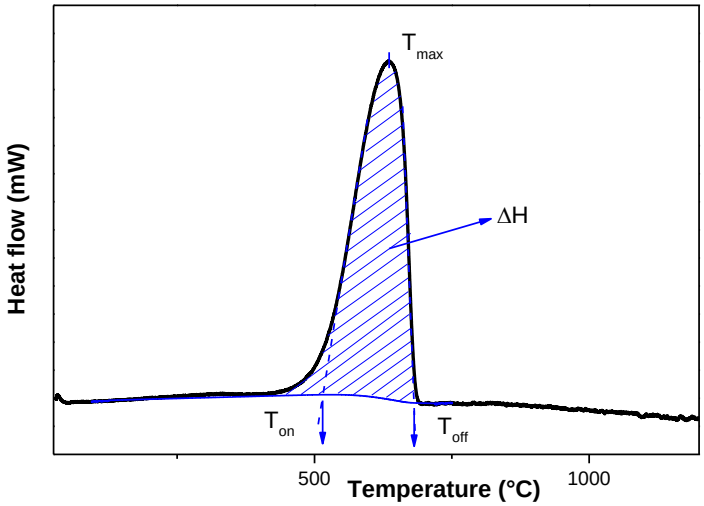

Table 3. Determination of T_{on}, T_{max} and T_{off} from the DSC curve.

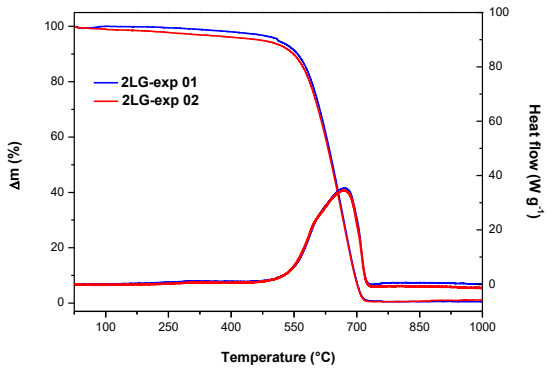
2LG-exp 01
2LG-exp 02
Δm (%)
Heat flow (W g-1)
Temperature (°C)

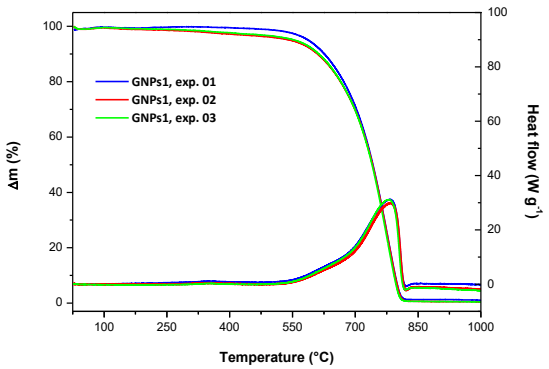
GNPs1, exp. 01
GNPs1, exp. 02
GNPs1, exp. 03
Δm (%)
Heat flow (W g-1)
Temperature (°C)

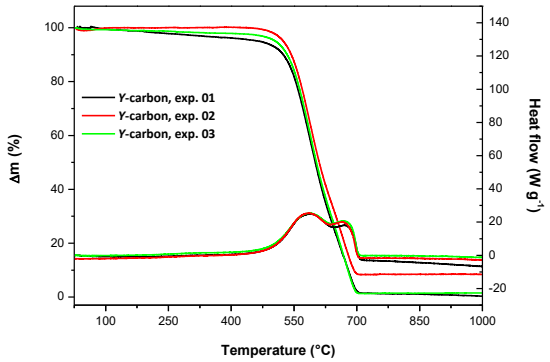
Y-carbon, exp. 01
Y-carbon, exp. 02
Y-carbon, exp. 03
Δm (%)
Heat flow (W g-1)
Temperature (°C)

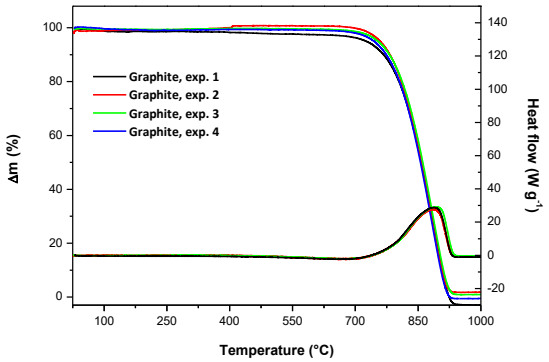
Graphite, exp. 1
Graphite, exp. 2
Graphite, exp. 3
Graphite, exp. 4
Δm (%)
Heat flow (W g-1)
Temperature (°C)

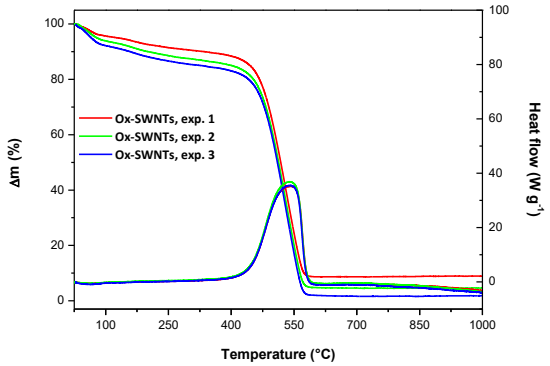
Ox-SWNTs, exp. 1
Ox-SWNTs, exp. 2
Ox-SWNTs, exp. 3
Δm (%)
Heat flow (W g-1)
Temperature (°C)

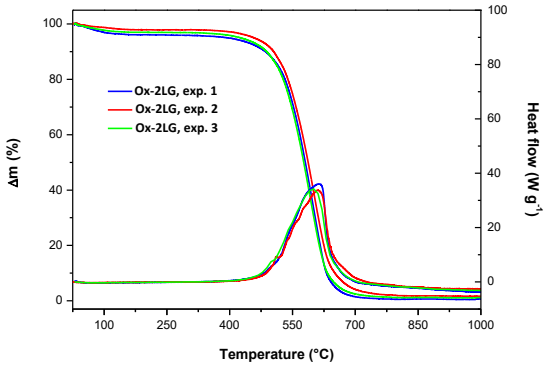
Ox-2LG, exp. 1
Ox-2LG, exp. 2
Ox-2LG, exp. 3
Δm (%)
Heat flow (W g-1)
Temperature (°C)

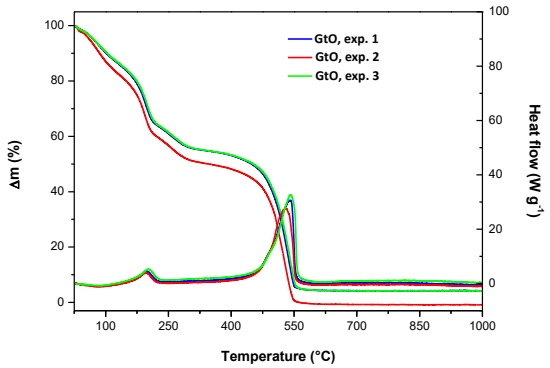
GtO, exp. 1
GtO, exp. 2
GtO, exp. 3
Δm (%)
Heat flow (W g-1)
Temperature (°C)

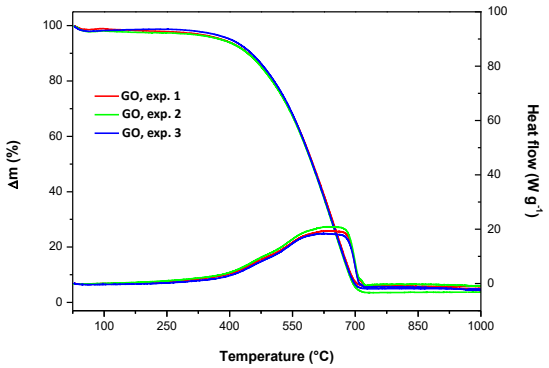
GO, exp. 1
GO, exp. 2
GO, exp. 3
Δm (%)
Heat flow (W g-1)
Temperature (°C)

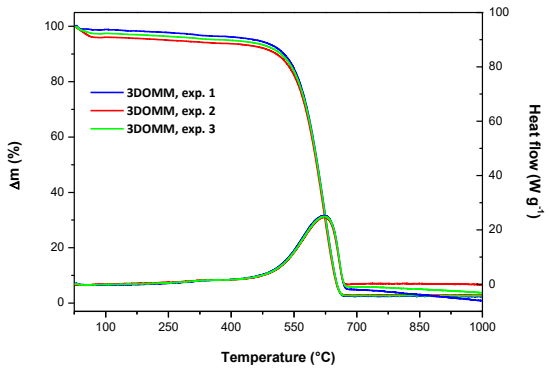

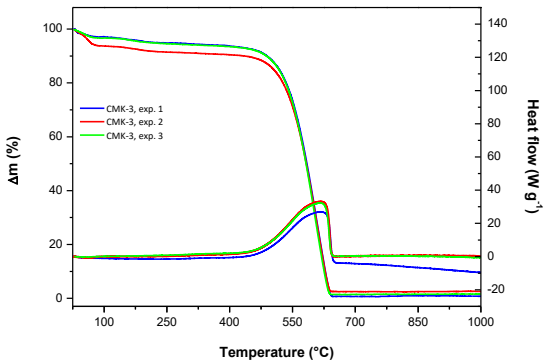

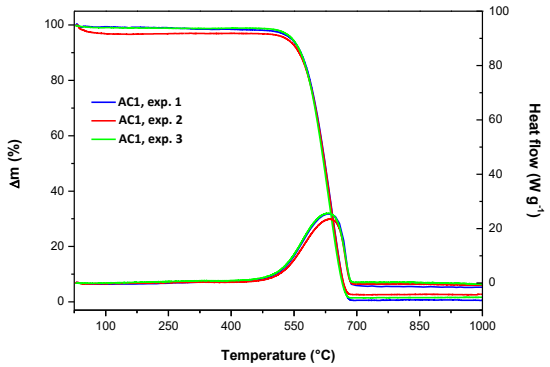

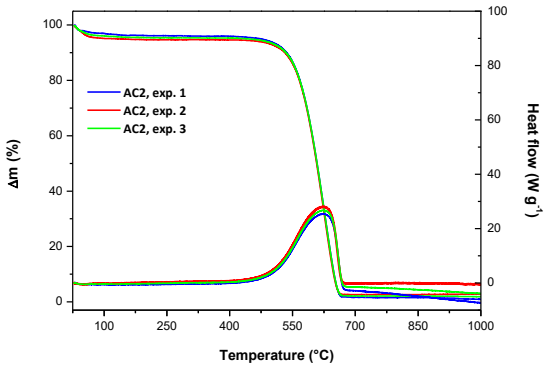

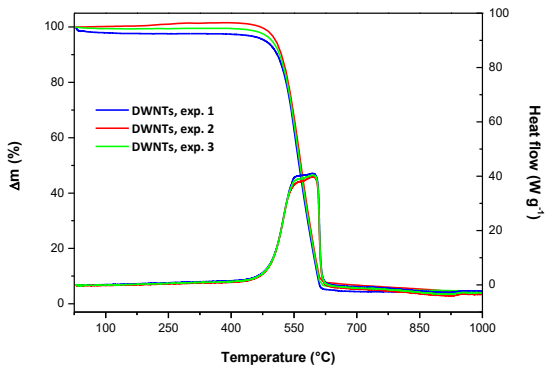

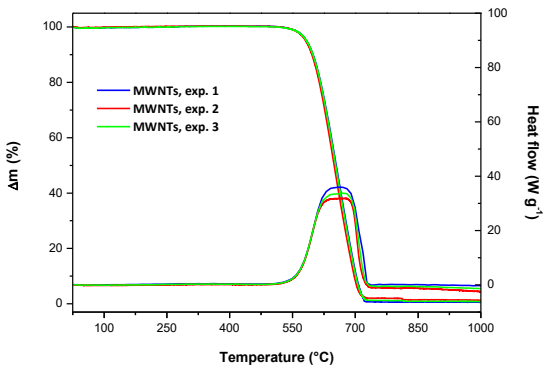

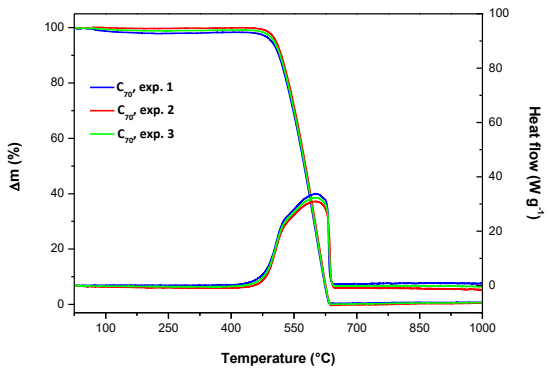

Table 4. Reproducibility of TG-DSC measurements.

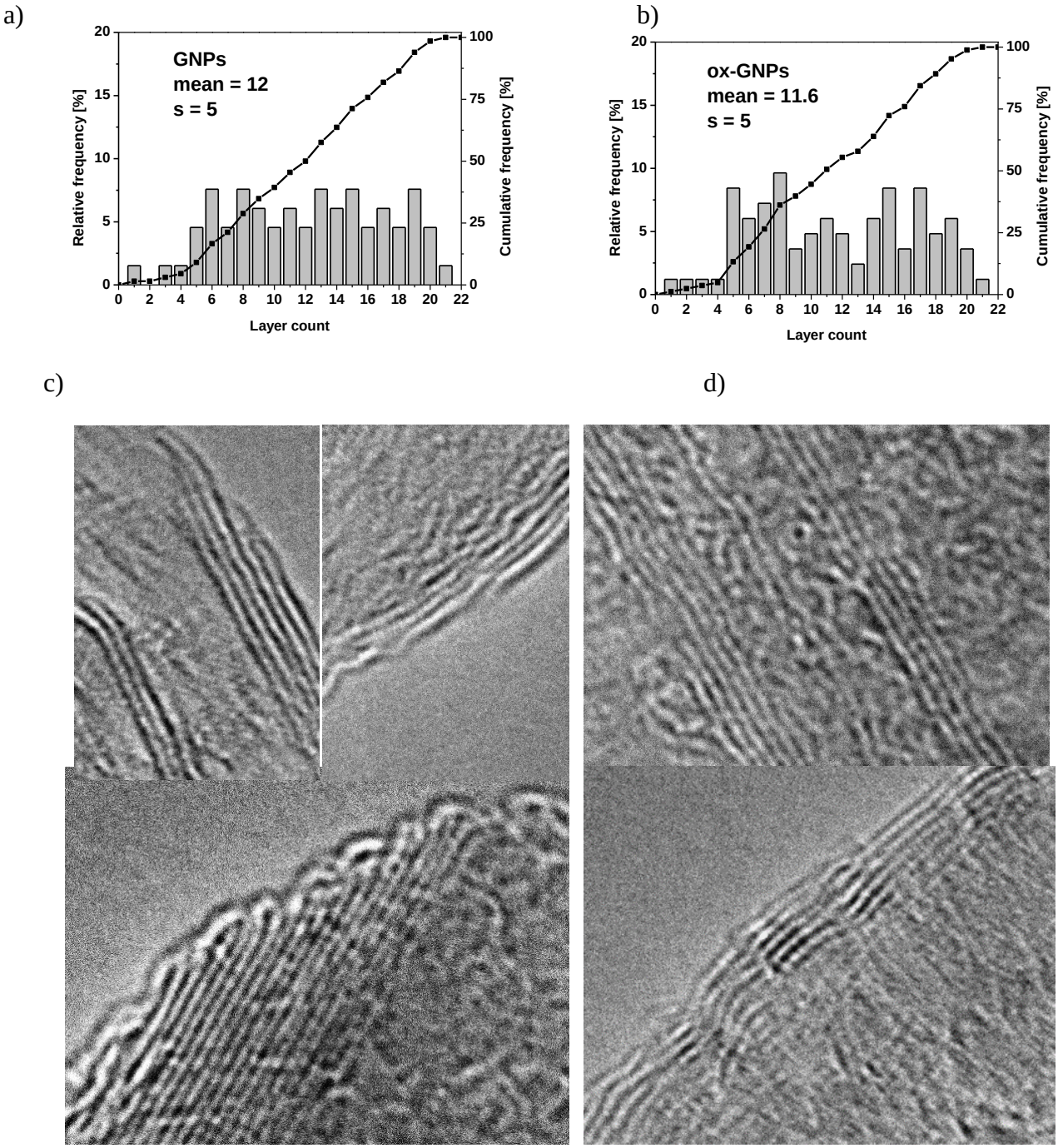

Table 5. Analysis of the number of layers in a) GNPs and b) Ox-GNPs and illustrative HRTEM images of c) GNPs and d) Ox-GNPs displaying the stacking of layers.

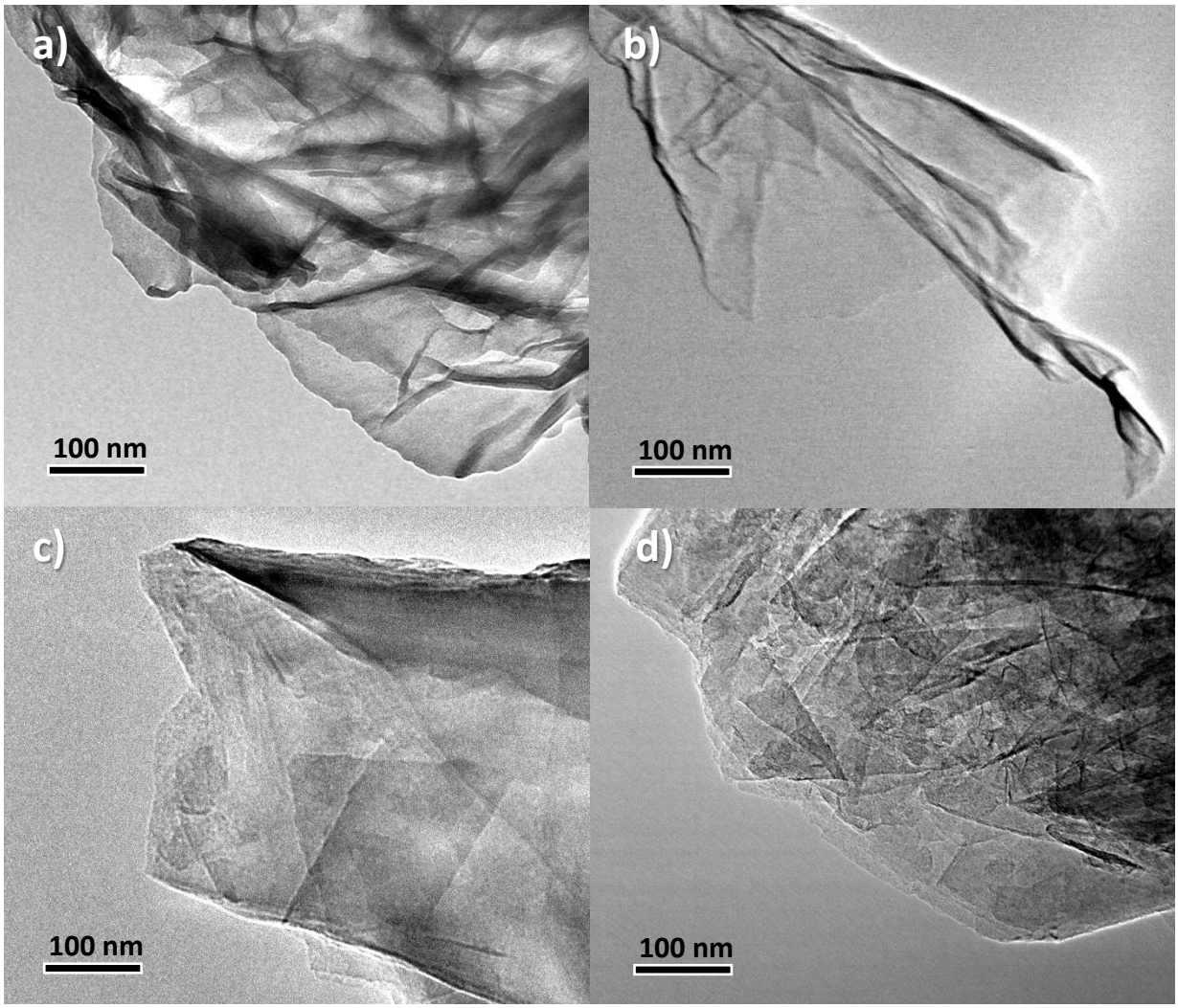

Table 6. Characteristic HRTEM images of a) Graphene, b) Oxidized double-layer graphene (Ox-2LG), c) Graphene nanoplatelets GNPs and d) Ox-GNPs at the same magnification.

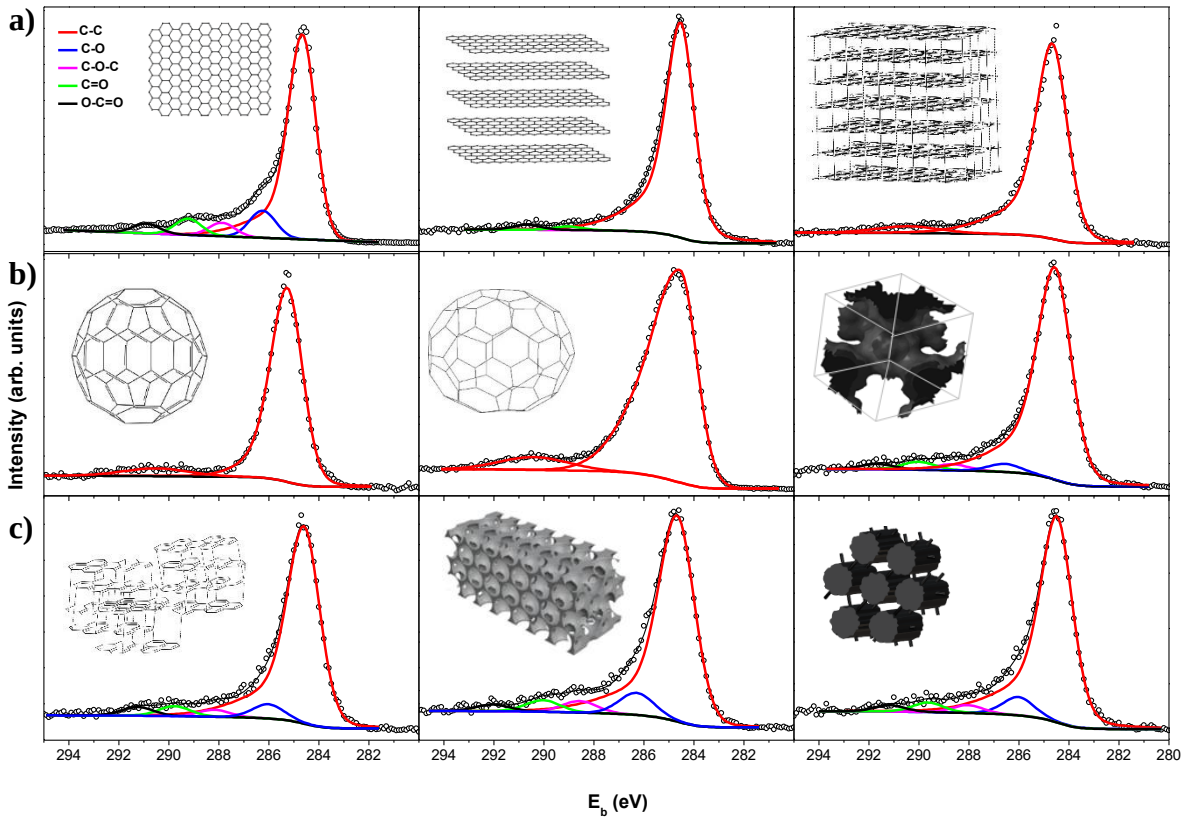

Table 7. Results of XPS spectra fitting into C and O chemical groups for a) planar carbon materials with different number of graphene layers, b) 3D carbon materials with a single graphene layer and c) amorphous and 3D organized mesoporous carbon materials.

Table S1. Assignment of oxygen containing functional groups of the samples by the values of Eb (eV) of (C 1s)x photoelectron lines as estimated by curve fitting of C 1s photoelectron spectra.

x	GtO	Ox-2LG	Ox-GNPs	Ox-SWNTs	mean [a]	Reference[b]	assignment
1	284.7	284.6	284.6	284.4	284.6 (0.13)	284.7 (0.24)	C-C
2	-	286.1	285.8	285.5	285.8 (0.30)	286.3 (0.40)	C-O
3	286.7	287.4	286.8	286.8	286.9 (0.32)	287.6 (0.07)	C-O-C
4	288.8	288.7	288.2	289.1	288.7 (0.37)	287.9 (0.14)	C=O
5	-	290.1	289.4	290.9	290.1 (0.75)	288.9 (0.22)	O-C=O

[a]numbers in brackets: standard deviation
[b]mean E_b values from refs. [1-5]

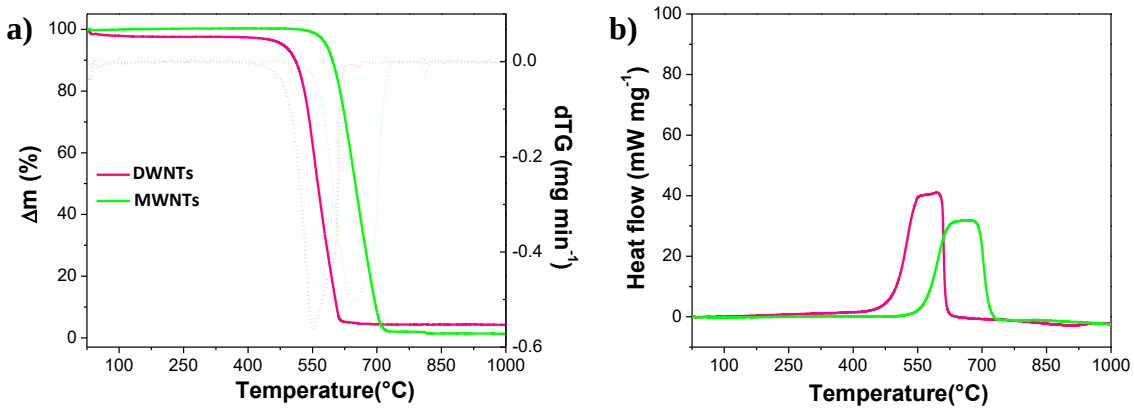

Table 8. TG/DTG-DSC analysis of thermal stability of a) DWNTs and b) MWNTs.

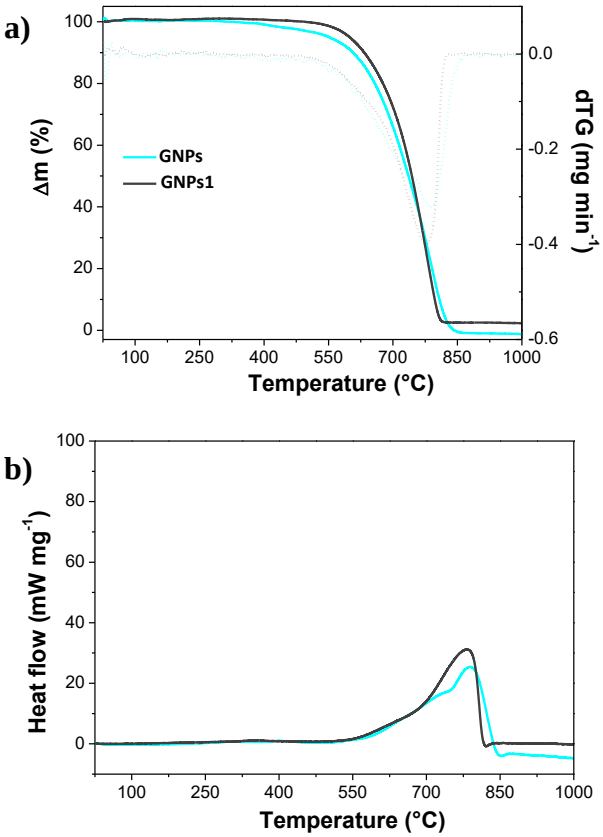

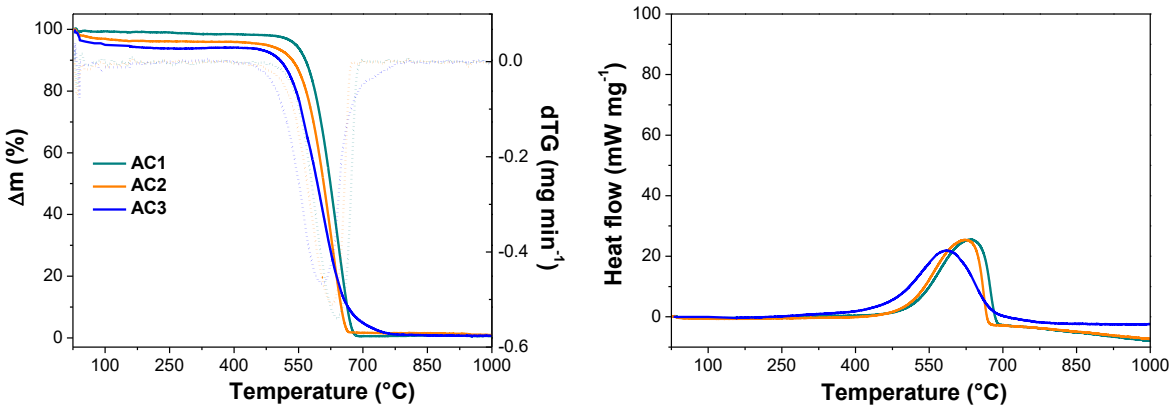

Table 9. TG/DTG-DSC analysis of thermal stability of multiple brands of a) GNPs and b) activated carbons.

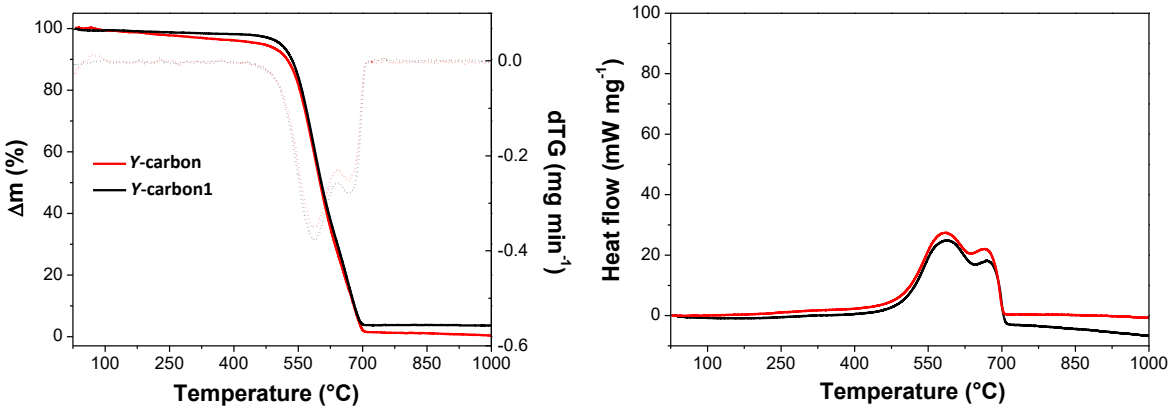

Table 10. TG/DSC Y-carbon from two different batch.

Table S2. DSC analysis of the thermal stability of carbon materials in air with the characteristic onset (T_{on}), maximum (T_{max}) and the offset (T_{off}) temperatures determined from the DSC signals.

Sample (Abbreviation)	T_{on} °C	T_{max} °C	T_{off} °C
Graphene nanoplatelets			
Graphene nanoplatelets, 15-20 layers (GNPs)	571±2	782±5	834±2
Graphene nanoplatelets (GNPs1)	638±1	777±1	815±1
Carbon nanotubes			
Oxidized single-walled nanotubes (Ox-SWNTs)	453±3	543±3	579±2
Double-walled nanotubes (DWNTs)	498±1	596±1	614±1

Multi-walled nanotubes (MWNTs)	569±2	654±5	721±5
Activated carbon			
Activated carbon 1 (AC1)	537±1	637±2	681±1
Activated carbon 2 (AC2)	527±1	624±1	668±1
Activated carbon 3 (AC3)	467±1	582±1	682±2
Zeolite templated replica			
Y-zeolite-templated carbon (*Y*-carbon)	496±5	587±1	707±2
		668±2	
Y-zeolite-templated carbon 1 (*Y*-carbon1)	515±5	591±1	706±2
		673±2	

References

[1] F.T. Johra, J.W. Lee, W.G. Jung, Facile and safe graphene preparation on solution based platform, J Ind Eng Chem 20(5) (2014) 2883-2887.
[2] R. Muzyka, S. Drewniak, T. Pustelny, M. Chrubasik, G. Gryglewicz, Characterization of Graphite Oxide and Reduced Graphene Oxide Obtained from Different Graphite Precursors and Oxidized by Different Methods Using Raman Spectroscopy, Materials 11(7) (2018) 1050.
[3] S. Park, J.H. An, I.W. Jung, R.D. Piner, S.J. An, X.S. Li, A. Velamakanni, R.S. Ruoff, Colloidal Suspensions of Highly Reduced Graphene Oxide in a Wide Variety of Organic Solvents, Nano Lett 9(4) (2009) 1593-1597.
[4] D. Yang, A. Velamakanni, G. Bozoklu, S. Park, M. Stoller, R.D. Piner, S. Stankovich, I. Jung, D.A. Field, C.A. Ventrice, R.S. Ruoff, Chemical analysis of graphene oxide films after heat and chemical treatments by X-ray photoelectron and Micro-Raman spectroscopy, Carbon 47(1) (2009) 145-152.
[5] R.B. Yi, X.M. Xia, R.J. Yang, R.S. Yu, F.F. Dai, J.L. Chen, W. Liu, M. Wu, J. Xu, L. Chen, Selective reduction of epoxy groups in graphene oxide membrane for ultrahigh water permeation, Carbon 172 (2021) 228-235.